



# Geology and evolution of fissure systems in fractured basement rocks, Calabria, southern Italy: implications for sub-unconformity reservoirs and aquifers

K. Hardman<sup>1,2</sup>, R. E. Holdsworth<sup>1,3\*</sup>, G. Palladino<sup>4</sup>, G. Prosser<sup>4</sup>, Z. Killingback<sup>1</sup> and K. J. W. McCaffrey<sup>1,3</sup>

<sup>1</sup> Department of Earth Sciences, Durham University, Durham DH1 3LE, UK

<sup>2</sup> Department of Geography, Geology, and Environment, University of Hull, Hull HU6 7RX, UK

<sup>3</sup> Geospatial Research Ltd, Durham DH1 4EL, UK

<sup>4</sup> Department of Sciences, Università degli Studi della Basilicata, 85-85100 Via Nazario Sauro, Potenza PZ, Italy

REH, 0000-0002-3467-835X

\* Correspondence: [r.e.holdsworth@durham.ac.uk](mailto:r.e.holdsworth@durham.ac.uk)

**Abstract:** Basement-hosted fissure-fill networks in sub-unconformity settings are increasingly recognized globally and have the potential to act as important subsurface reservoirs and/or migration pathways for hydrocarbons, geothermal fluids and groundwater. We examine well-exposed fissures from exhumed crystalline upper Carboniferous basement rocks in southern Italy (Calabria) and describe their nature, origin and evolution. The basement rocks record the emplacement and exhumation of their plutonic protoliths. The evolution of these rocks includes their initial intrusion in the late Carboniferous, followed by veining, folding and rifting events, to eventual exhumation at the surface when fissuring occurred in the mid-Miocene. The fissure network hosts fossiliferous marine sediments, wall rock collapse breccias and limited mineralization with vuggy cavities. In the basement below the main erosional unconformity, fissure-fills form up to 50% by volume of the exposed rock. The fills are notably more porous (up to 15–25% matrix porosity) than the ultra-low-porosity (<1%) crystalline host rocks. We present field observations, palaeostress analyses of fault slickenlines and fracture topology analyses demonstrating that these exceptionally well-connected fissure networks are related to rifting and penetrated to depths of at least 150 m below the main Miocene erosion surface.

Received 6 June 2022; revised 15 December 2022; accepted 22 December 2022

Recent field-based geological studies have highlighted the importance of near-surface fault and fissure development in low-permeability rocks, such as basalts, limestones, mudstones and crystalline basement (e.g. Walker *et al.* 2011; Woodcock *et al.* 2014; Palladino *et al.* 2016, 2018; Hardman *et al.* 2020; Holdsworth *et al.* 2020; Ceccato *et al.* 2021). These partially open fractures, which may contain wall rock breccia, sedimentary material or hydrothermal mineralization, are thought to substantially enhance the reservoir storage and transport properties of groundwater, hydrocarbons, magma and hydrothermal fluids in otherwise very low permeability host rocks (e.g. Gutmanis 2009; Trice 2014). These structures are therefore of key interest in the assessment of subsurface geological resources and can also shed new light on active rifting processes, including seismicity (Holdsworth *et al.* 2019; Hardman *et al.* 2020).

Well-exposed examples of fissured basement rocks are preserved in the coastal outcrops of Calabria, southern Italy (Figs 1a and 2; at Copanello, Pietragrande and Palmi). These belong to a suite of regionally recognized networks of sediment-filled fissures seen cutting basement rocks across Calabria and Sicily (e.g. Montenat *et al.* 1991). In all areas, the modern surface topography and coastal processes have preserved exceptional 3D exposures of the basement rocks and lowermost Miocene–Pliocene fills related to adjacent younger Cenozoic basins, such as the Crotona Basin (Zecchin *et al.* 2012).

We present field and microscopic observations, structural data, palaeostress inversion analyses and virtual outcrop studies from fissure-filled fractures and the pre-existing basement fabrics and fault rocks. We show that highly interconnected, porous fissure-fill networks can constitute a substantial proportion of the local rock

volume in basement below regional unconformities and may exhibit and preserve exceptional reservoir properties through geological time. These findings have important global implications for the hydrodynamic properties and economic potential of up-faulted, sub-unconformity crystalline basement blocks – the so-called ‘buried hill’ reservoirs (e.g. Biddle and Wielchowsky 1994; Cuong and Warren 2009).

## Geological setting

The Calabria–Peloritani terrane in southern Italy (Fig. 1b) is a detached orogenic arc–basement complex separating the subducting Ionian lithosphere to the SE from the Tyrrhenian lithosphere to the NW (Fig. 1c) (Finetti and Del Ben 1986). This *c.* 230 km long overriding continental complex stretches from mid-Sicily to the Sila mountains. The crust of the Calabrian arc terrane consists of granulite to greenschist facies Paleozoic metamorphic rocks intruded by Permo-Carboniferous granitoids (Caggianelli *et al.* 2000; Van Dijk *et al.* 2000; Langone *et al.* 2014; Ortolano *et al.* 2020). The intrusions form a series of elevated regions in southern Italy, including the Aspromonte, Serre and Sila massifs (Fig. 1a). The plutons and surrounding host rocks were involved in a Cretaceous to Paleogene Calabria–Peloritani orogenic event and were then progressively exhumed and uplifted during the late Eocene–Oligocene to form a chain of mountains >1 km high (Fig. 1b; Thomson 1994; Bonardi *et al.* 2001; Cirrincione *et al.* 2015; Ortolano *et al.* 2020).

In the mid- to late Miocene (Tortonian–Messinian), following Oligocene uplift, the Calabrian complex underwent NW–SE extension, forming a series of back-arc transtensional NE- and

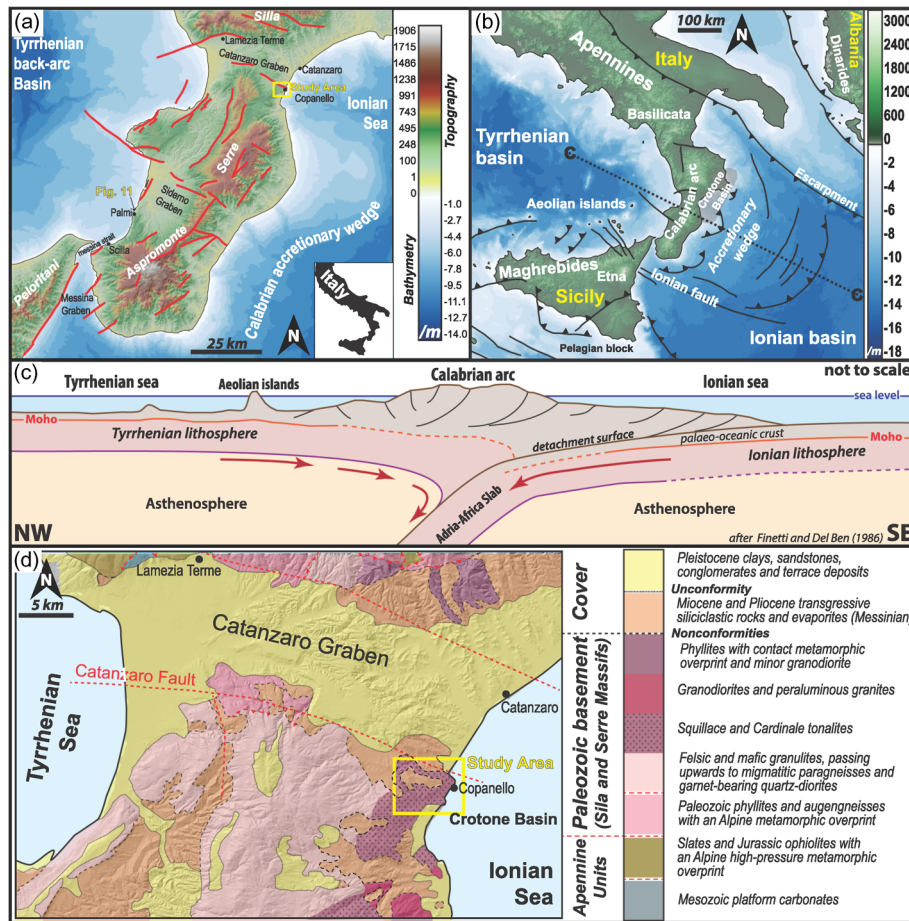


**Fig. 1.** Location and tectonic setting of the study area. **(a)** Topographic and bathymetric map of Calabria showing the key mountain ranges/massifs and basins. Inset shows the location of the study area in Italy; the location of Figure 11 is indicated on the main map. **(b)** Tectonic map of southern Italy and Sicily. The location of the cross-section in part (c) and the Crotona Basin are also shown. **(c)** Cross-section showing the subduction of the Ionian lithosphere under the Tyrrhenian lithosphere beneath the Calabrian arc. **(d)** Regional geological map of the Catanzaro graben and northern Serre Massifs showing regional basement–cover relationships. Source: (c) Finetti and Del Ben (1986).

NW-trending fault-bounded basins associated with the opening of the Tyrrhenian Sea (Thomson 1994; Monaco *et al.* 1996; Brutto *et al.* 2016). Near to the present study area, the opening of the Crotona forearc basin to the SE (Massari and Prosser 2013) marked a transition from orogenic uplift and back-arc extension to forearc extension and was associated with the deposition of a Serravallian–Late Messinian stratigraphic sequence, bounded at its base by a top-basement erosion surface and upwards by a regional unconformity known as the Messinian Erosional Surface (MES; Fig. 1d) (Zecchin *et al.* 2012; Cornée *et al.* 2016).

Within the core of the Calabrian complex, mid-Miocene tectonic extension was accommodated by a series of NW-oriented transtensional faults (Fig. 1a). These large sinistral-normal oblique-slip faults bound the Catanzaro, Siderno and Messina graben, which separate the Serre, Silla Aspromonte massifs and the Peloritani mountains (Fig. 1a, d) (Monaco *et al.* 1996; Van Dijk *et al.* 2000; Spina *et al.* 2011; Brutto *et al.* 2016). Tectonism has continued, with evidence for WNW–ESE extension in the middle Pleistocene, and Recent seismicity associated with exposed NW-dipping rupture surfaces along the Sant’Eufemia, Cittanova and Serre faults (Minelli *et al.* 2016; Tripodi *et al.* 2018).

As a result of this tectonically long-lived deformation, the Calabrian crystalline basement complex located close to the basal Cenozoic erosion surface has been intensely faulted and fractured. It is well exposed on the coast, where it forms an outstanding natural laboratory for the study of sub-unconformity basement structures.

### Field and laboratory methods

Localities were studied along the Copanello and Pietragrande coastline, where fracture systems and their associated fills are very well exposed in the tonalite basement that underlies the regional

base-Miocene unconformity. A further set of fissure-fills was briefly studied at Palmi in similar basement rocks exposed near to the Straits of Messina on the western coast of Calabria. The fissure systems are typically highlighted by the presence of pale yellow/grey sands infilling the light grey felsic host rocks. Given the significant topography in the study areas (elevations extend from sea-level to 120 m, with individual cliffs up to 70 m high), this provides an opportunity to study the structures at different elevations as a proxy for different depths within the basement below the regional unconformity.

Structural geometries were recorded through field observations and the collection of orientation data, with fault kinematics measured from offset markers, localized slickenline lineations and local asymmetrical shear criteria, such as jogs and the development of Riedel shears (Petit 1987). The relative ages of fractures and their fills were determined using cross-cutting relationships that can be correlated between outcrops. In selected well-exposed rock platforms, low-altitude aerial images were collected using an unmanned aerial vehicle Quadcopter (DJI Mavic Pro with a gyroscopically mounted 13.1 MP camera). Where appropriate, representative samples of oriented hand specimens were collected from the host rocks, fault rocks and mineral/sediment fills of fractures. These were sectioned and then impregnated with blue resin to highlight the porosity, which was estimated by eye using transmitted light optical microscopy. This also allowed the microstructure and relative age relationships of fracturing, mineralization and cementation to be determined.

Having subdivided the brittle structures into different relative age groups based on cross-cutting relationships and kinematic shear criteria, palaeostress inversion techniques were used for faults where slickenlines are preserved to determine an approximation of the stress conditions responsible for their formation. This was



The tonalite basement is unconformably overlain by a marine sedimentary sequence with a basal chaotic clast-supported conglomerate (Fig. 2c; Siddoway *et al.* 2019). This top-basement erosion surface is hereafter referred to as the ‘main erosional unconformity’. The clasts consist exclusively of rounded grains (mm) to boulders (m) of igneous rocks (tonalite, mafic enclaves and aplite) and subordinate amounts of Paleozoic metamorphic rock types set in a fine- to medium-sized sandy matrix. Previous researchers (Siddoway *et al.* 2019) have highlighted the similarity of the conglomerate with the coarse-grained deposits occurring at the base of the upper Serravallian–Tortonian San Nicola Formation, widely exposed in the Croton Basin (Van Dijk *et al.* 2000; Massari *et al.* 2010; Massari and Prosser 2013). Regionally, the San Nicola Formation consists of upwards-fining sediment packages passing from pebble and boulder conglomerates and braided coastal deposits at the base of the succession up into arkosic marine shoreface sandstones at the top (Massari *et al.* 2010; Massari and Prosser 2013).

The basal conglomerate is overlain by a finer grained microbreccia (Fig. 2d). It is typically a chaotic aggregate of small angular grains of tonalitic and detrital fossiliferous material set in a crystalline calcite matrix; interstitial calcareous muds are absent. Rind-like calcite cements rarely fill all the available intergrain pore spaces, resulting in an exceptionally high porosity (30–40%). This horizon has previously been interpreted as a shallow marine coastal fan or proximal braided stream deposit of the San Nicola Formation (Massari *et al.* 2010; Massari and Prosser 2013).

Collectively, the basal conglomerates and microbreccias vary significantly in thickness from zero to tens of metres and pass conformably up into sandstones, forming the upper part of the San Nicola Formation (Massari *et al.* 2010; Siddoway *et al.* 2019). This unit further infills the irregular basement topography and varies in thickness from nearly zero to 90 m, reaching its thickest values where it lies in local palaeotopographic lows. The pale yellow/grey sandstones consist of 0.2–0.5 mm rounded grains of mainly plagioclase and quartz sourced from the basement rocks (Fig. 2e; Massari *et al.* 2010; Massari and Prosser 2013). A variety of fragmented fossiliferous materials are found in these clastic rocks, including bryozoa, pectinids, bivalves and corals (Fig. 2e).

Conformably overlying the San Nicola Formation regionally are Tortonian shales and clays of the Ponda Formation, although these are only locally present in the study area as a <1 m thick shale horizon, which is truncated by the overlying unconformity at the base of the Messinian limestones (the MES). The Ponda Formation clays are soft, white diatomaceous clays and silts, interpreted to have formed in a low-oxygenated outer shelf environment (Massari and Prosser 2013). The overlying Messinian limestones (Fig. 2f) are a tens of metres thick sequence of pale yellow/brown coloured vacuolar evaporitic limestones (Van Dijk *et al.* 2000), with local stromatolitic structures and thin intercalations of silty to sandy siliciclastic material (Guido *et al.* 2007; Massari *et al.* 2010).

## Basement structural history

### Magmatic deformation

In the study area, metre- to kilometre-thick sheets of amphibole- or biotite-rich tonalite and granodiorite form 90–95% of the basement lithologies, while the remaining 5–10% consist of dioritic and gabbroic enclaves (Fig. 3a; percentages based on visual estimates made in the field). A weak alignment of the constituent minerals lies sub-parallel to the sheeted boundaries and, viewed in thin section, an absence of solid-state recrystallization textures suggests that the foliation is a magmatic-state deformation fabric (Hutton 1988; Tribe and D’Lemos 1996). The lozenge-shaped mafic enclaves are also deformed, with their long axes oriented parallel to the foliation and

magmatic banding, with local evidence for flow banding and schlieren textures wrapping around the enclaves (Fig. 3a). Both the foliation and compositional sheeting display a regionally consistent, steeply SE-dipping orientation (mean 029/61 SE), which is oriented parallel to the trend of both the Calabrian arc and the Ionian subduction zone (Figs 2b, 3a).

### Ductile shears and folds

At Pietragrande (38° 45′ 11.9″ N, 16° 34′ 06.5″ E), small (<5 cm wide) ductile shear zones are developed along some compositional contacts between leucocratic and melanocratic bands (Fig. 3b). These are cross-cut by local pegmatite and aplite veins. Given the sparsity of the shear zones and the lack of clear shear sense indicators, it is not possible to determine the significance of this deformation in the field. However, work in the Serre region and adjacent Sila Massif to the north (Fig. 1a) has described a phase of 650–550°C solid-state deformation related to post-emplacement extension (Caggianelli *et al.* 2000; Langone *et al.* 2014). The rocks at Pietragrande also feature metre-scale, shallowly south-plunging open folds of the sheeted units and mafic enclaves with gently west-dipping axial surfaces (Fig. 3b).

### Pegmatite and aplite veining

There are widespread cross-cutting veins of pale white pegmatite and aplite (Fig. 3c), consisting almost exclusively of quartz and feldspar. The vein widths vary from a few centimetres up to a metre, with sharply defined margins (Fig. 3c). They lack internal deformation fabrics and probably represent a magmatic feature formed prior to complete cooling of the plutonic complex.

Within the study area, the pegmatites and aplite veins are oriented sub-parallel to one another, but cross-cut the SE-dipping magmatic foliation and compositional banding, striking NNE–SSW with a subvertical to steep WNW dip (mean 195/66 WNW) (Fig. 3c). Offset markers across the vein margins show that these veins are tensile, suggesting an ESE–WNW extension direction during emplacement.

### Cataclasis and frictional melting

Brittle faults hosting mutually cross-cutting epidote-mineralized cataclasites and sub-parallel pseudotachylytes (Fig. 4a) display predominantly extensional offsets of compositional markers, pegmatite and aplite veins (Figs 3d, 4a; Caggianelli *et al.* 2005). The faults form as new cross-cutting features, but also locally reactivate older structures, leading to a complex array of interconnected faults with a spread of orientations (Fig. 3d). Overall, the majority of pseudotachylyte- and cataclasite-hosting faults trend NNE–SSW, with a moderate ENE or WSW dip of 30–80°. A secondary set of broadly ESE–WNW faults moderately dipping south (20–60°) is also present (Fig. 3d). Overall extensional movements are indicated by the preservation of slickenlines, with shear senses given by the preservation of offset markers, the sigmoidal wrapping of clasts, an echelon quartz-filled tension gashes, Riedel shears and dilational jogs (Fig. 4b, c). The regional extension direction associated with these structures is east–west (Fig. 3d).

The fault-hosted foliated cataclasites are typically <50 cm thick. The fragmentation, alignment and brittle dismemberment of quartz and plagioclase crystals can be seen with the naked eye. They characteristically display pervasive retrograde growth of pale green epidote (after plagioclase) and dark green chlorite (after biotite).

The pseudotachylytes are characteristically associated with perpendicular tensile injection veins emanating from the shear surface where the frictional melt is probably generated (Figs 3d, 4d;

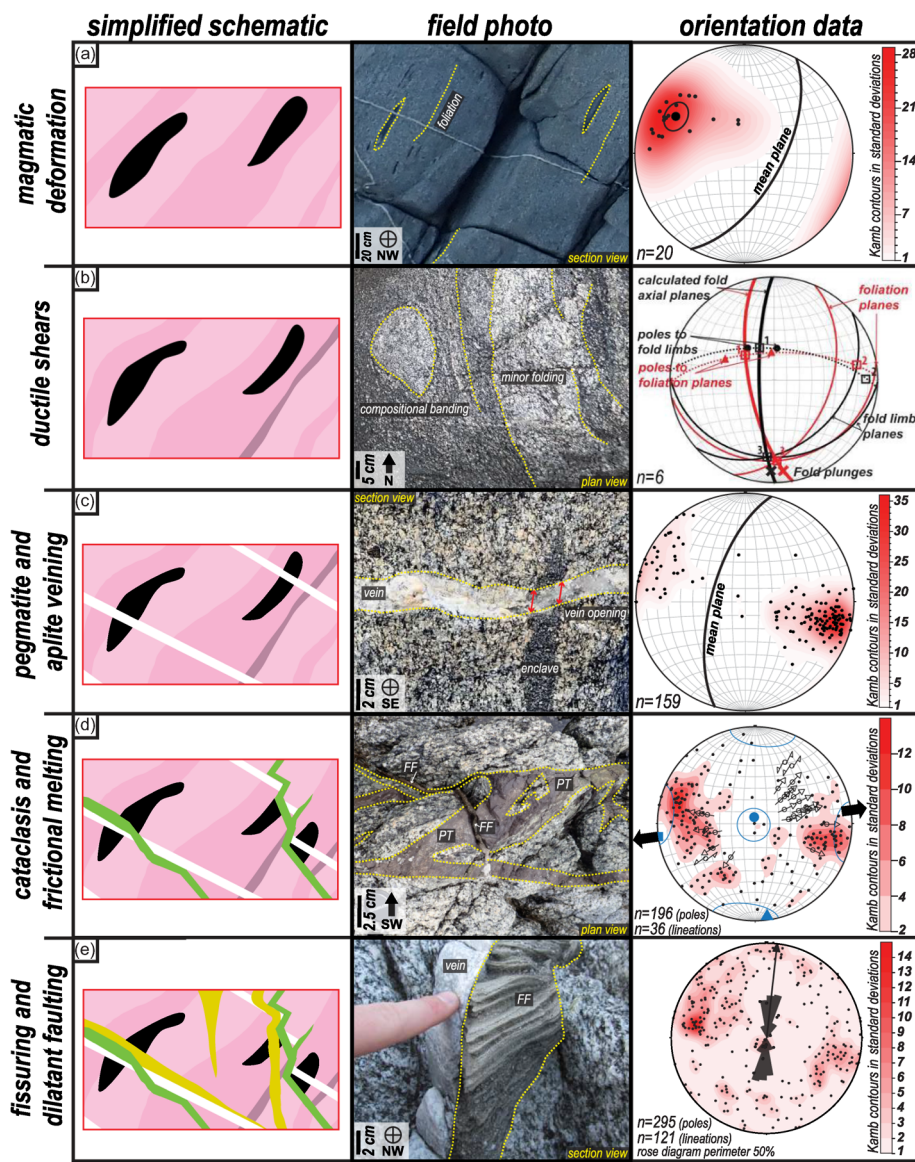


**Fig. 3.** Summary tectonic history and fabrics of the Serre Batholith. All parts show a simplified model (left-hand panel), field photograph (centre panel) and stereographic projection (right-hand panel). (a) Early magmatic deformation of the basement, including a foliation, elongate mafic enclaves and compositional banding ( $38^{\circ} 45' 35.4''$  N,  $16^{\circ} 34' 18.9''$  E). (b) Early ductile shearing and minor folding of the basement ( $38^{\circ} 45' 47.4''$  N,  $16^{\circ} 34' 09.8''$  E). (c) Apatite and pegmatite veining showing dilatant offsets picked out by enclave offset ( $38^{\circ} 45' 34.3''$  N,  $16^{\circ} 34' 18.3''$  E). (d) Deep brittle shears including chloritized cataclasite and frictional melts – pseudotachylytes cut by a later fissure-fill ( $38^{\circ} 45' 44.0''$  N,  $16^{\circ} 34' 11.9''$  E). (e) Near-surface fissuring and infilling with pale bedded sediment ( $38^{\circ} 45' 34.0''$  N,  $16^{\circ} 34' 18.2''$  E). Rose diagram superimposed on stereographic projection summarizes dilation vector data showing north–south opening of fissures. FF, Fissure-fill; PT, pseudotachylyte.

Rowe *et al.* 2018). These veins of frictional melt reach thicknesses of up to 20 cm and can occur in networks of multiple sub-parallel interlinked melting/slip surfaces within one fault zone (Figs 3d, 4a). A glassy matrix of dark brown–black aphanitic glass typically hosts clasts of rounded country rock (Figs 3d, 4a, d). In thin section, many pseudotachylyte veins show a distinct zonation, with a flow-banded darker cryptocrystalline spherulitic matrix at the fault margins and a lighter microlitic matrix in the centre (Fig. 4e, f).

### Shallow fissuring and dilatant faulting

The youngest structures present in the study area are locally extensive sets of interconnected breccia- and sediment-filled fractures and faults (Fig. 3e). These features occur pervasively within the basement tonalite as well as in the overlying conglomerate and microbreccia units. The fills typically consist of brecciated wall rock, pale sandstone, rounded boulders of tonalitic host rock and detrital fossiliferous material (Fig. 3e). The fills commonly feature sedimentary structures and are interpreted to have formed at or close to the Miocene palaeosurface (i.e. the main erosional unconformity) and are referred to hereafter as ‘fissures’.

The fissures show a variety of orientations that include sets striking NNE–SSW where they have reactivated foliation planes, vein margins and cataclasites. Kinematic data from fissures measured from offset markers yield dilation vectors with a strong

north–south trend. Thus, despite the broad range of fissure orientations, they seem to share a regionally consistent opening direction (Fig. 3e), which lies orthogonal to that determined for the older cataclasite- and pseudotachylyte-bearing faults. Most fissures have apertures of  $<30$  cm, but multi-metre wide examples exist at Copanello South ( $38^{\circ} 45' 26.4''$  N,  $16^{\circ} 34' 10.1''$  E) and North ( $38^{\circ} 45' 47.4''$  N,  $16^{\circ} 34' 09.6''$  E). Given that the sedimentary fills include fossils, it is reasonable to assume that these dilatant fissures were infilled from above following their formation at or near the palaeosurface.

### Later faults

Across the study area, sporadic larger offset faults are observed and inferred to cross-cut the basement, Miocene sequences and overlying Messinian–Pliocene strata (Fig. 2). The faults have decametre offsets and trend either ENE–WSW (parallel to the nearby Catanzaro Fault) or NE–SW (Fig. 2). As a result of the lack of exposure, it is unclear whether these faults reactivate any earlier structures or carry any slip-vector data. Ongoing seismic activity in the region (e.g. Minelli *et al.* 2016; Tripodi *et al.* 2018) has been attributed to forearc rifting in the Ionian Sea and the opening of the offshore Croton Basin (Zecchin *et al.* 2012). The sedimentary successions exposed in the Croton Basin record cyclical phases of uplift during the mid-Pliocene, early Gelasian, mid-Pleistocene, late

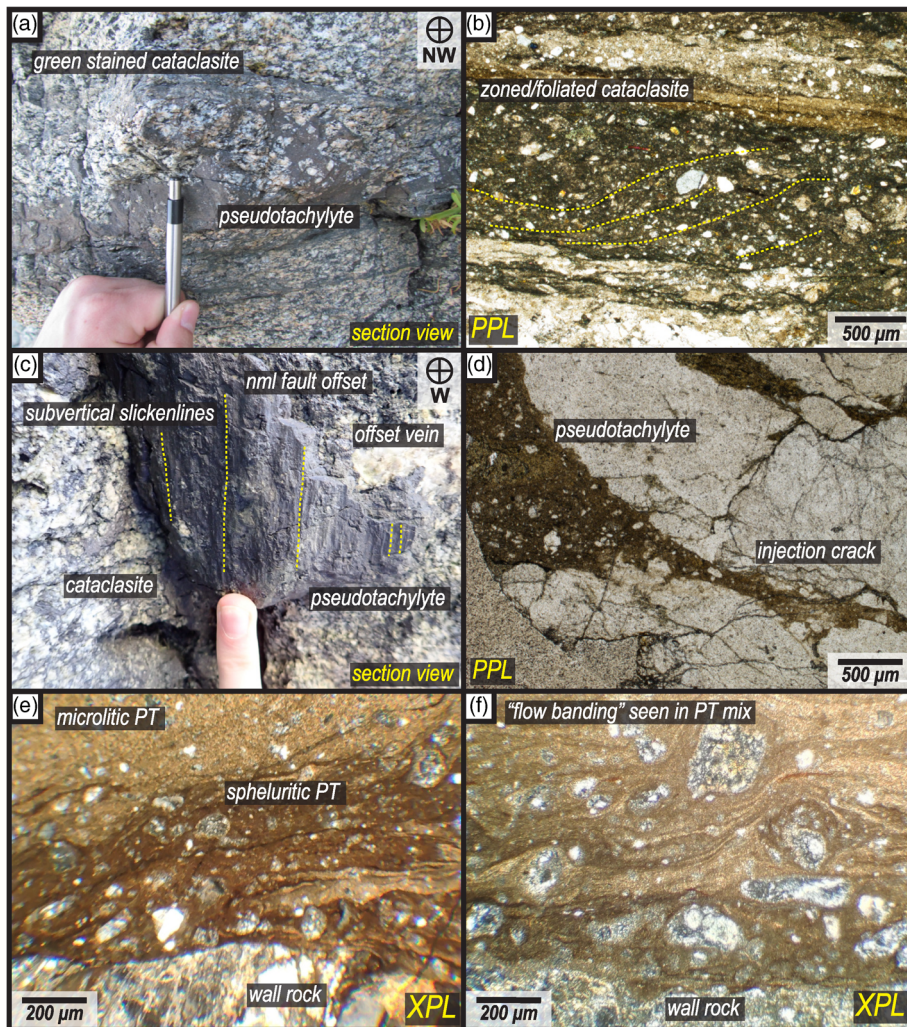


**Fig. 4.** Field and microstructural fabrics related to the cataclasite- and pseudotachylyte-bearing faults. (a) Field photograph showing pseudotachylyte injection veins cross-cutting and caught between two green-stained chloritized cataclastic faults (38° 45' 41.9" N, 16° 34' 16.4" E). (b) Thin section photomicrograph in plain polarized light showing zoned and foliated cataclasite. (c) Field photograph of pseudotachylyte hosting fault with subvertical slickenline striae (38° 45' 41.9" N, 16° 34' 16.4" E). The abbreviation nml means normal. (d) Thin section photomicrograph in plain polarized light of pseudotachylyte injection vein with an injection/'wing' crack. (e) Thin section photomicrograph in cross-polarized light of pseudotachylyte banding at the wall rock interface with microlitic paler melts with smaller clasts and darker, finer spheluritic melts with larger and more frequent clasts at the fault margins. (f) Thin section photomicrograph in cross-polarized light of asymmetrical banding/flow structures around clasts in frictional melts along the wall rock interface. PT, pseudotachylyte.

Ionian and Recent, interspersed between phases of subsidence and the accumulation of sediments (Zecchin *et al.* 2012).

## Fissure architectures

### Copanello North

A very well-exposed, 500 m long NW–SE-trending coastal platform occurs between 38° 45' 49.1" N, 16° 34' 08.6" E and 38° 45' 34.4" N, 16° 34' 17.5" E. Basement tonalite is continuously exposed, with smaller outcrops of overlying conglomerate, microbreccia and Messinian carbonates (Figs 2, 5a–c). The platform is cut by three unexposed NE–SW-trending normal faults, the presence of which can be inferred from offsets of the mapped geological units (Fig. 2). Collectively, the faults form a graben–horst basement topography within which the conglomerate and microbreccia cover sequences were deposited. This fault-controlled palaeotopography probably accounts for the present day lateral discontinuity of the units, with apparent thickening of strata close to the normal faults. The northernmost structure, which lies closest to the Catanzaro Fault, is larger, with a throw of 50–60 m cutting multiple units including the basement, a >5 m wide NW–SE-trending sediment-filled fissure and the overlying Messinian cover.

Sediment-filled fissures can be found throughout this section of coastline, predominantly within the tonalite (Fig. 5d–f), but also cutting the overlying basal conglomerate and microbreccia sequences (Fig. 5b). A mutually cross-cutting relationship between these sedimentary sequences and the sediment-filled fissures is preserved locally and is best observed at 38° 45' 36.9" N, 16° 34' 16.6" E.

The sediment-filled fissures that have not reactivated pre-existing structures exhibit a wide spread of orientations, with vertical to horizontal fractures present (Fig. 5g). Subvertical members of this group show a clustering of ENE and NNE trends, with a further sub-horizontal cluster developed. The fissures display a mean opening vector of  $006.3^\circ \pm 3.1^\circ$  based on offset markers (Fig. 5g), but few east–west-striking fissures are observed. Instead, the broadly orthogonal clusters of fissures suggest that these 'virgin' fissures may follow pre-existing orthogonal cooling joints within the pluton, although no unequivocal evidence for the existence of these joints could be found. The connectivity of the fissure network is high in all directions and can be quantified using fracture topology (Sanderson and Nixon 2015). For example, analysis of the sample areas shown in Figure 5i shows branch line ratios  $>2.0$ , with a mean of 4.2, and an average connections/branch ratio of 1.99, with a consistent dominance of T nodes over I or X nodes (Fig. 5i, Table 1). This demonstrates that the fissure systems here are exceptionally well connected.

The sediment-filled fissures at Copanello North have a mean aperture of 40.4 cm, with a range from  $<0.5$  to  $>200$  cm (Fig. 5h). Here, we refer to 'aperture' as the opening component of displacement, including the fill (the 'kinematic aperture' of Ortega *et al.* 2006). The data collected from Copanello North, and across the whole study area, appear to show power law scaling relationships similar to those determined elsewhere by Ortega *et al.* (2006) and McCaffrey *et al.* (2020) (Fig. 5h; see Hardman 2020).

The spatial distribution of sediment-filled fissures shows no clear increase in intensity, size or aperture northwards towards the Catanzaro Fault. Here, the primary control on fissure intensity along the coastline is exposure – the largest accumulations of fissures and

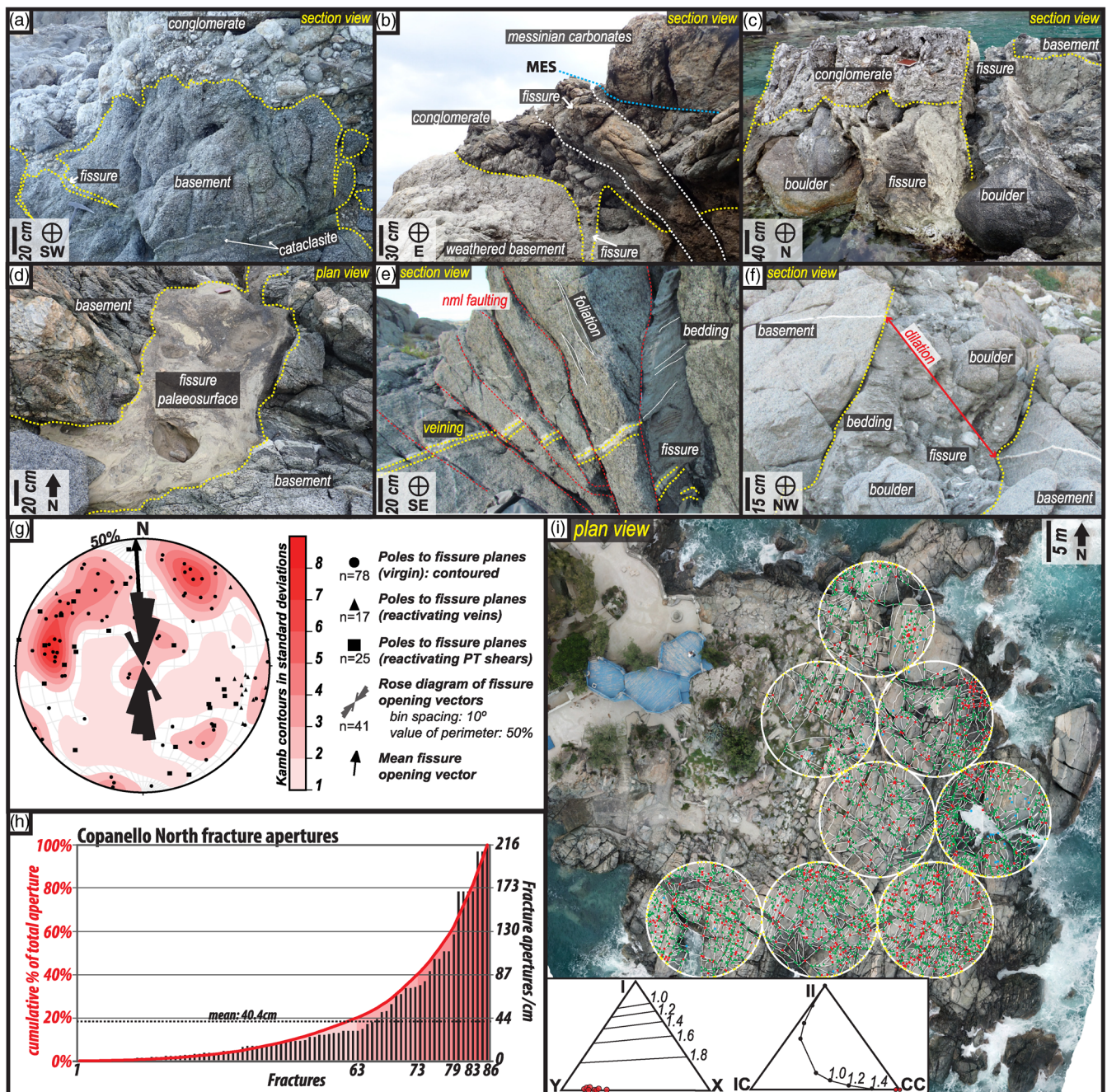


**Fig. 5.** Copanello North locality. (a) Field photograph showing erosive contact between unweathered basement and basal conglomerate highlighted in yellow ( $38^{\circ} 45' 37.4''$  N,  $16^{\circ} 34' 15.9''$  E). Note minor fissures filled with finer material from the conglomeratic matrix. (b) Field photograph showing basal stratigraphic relationships between the weathered basement, basal conglomerate, Messinian carbonates and cross-cutting fissures ( $38^{\circ} 45' 41.9''$  N,  $16^{\circ} 34' 16.4''$  E). (c) Field photograph showing a major fissure-fill filled with large boulders, overlain by basal conglomerate and both cut by a later fissure-fill ( $38^{\circ} 45' 47.4''$  N,  $16^{\circ} 34' 09.7''$  E). (d) Field photographs showing an exposed palaeosurface from a wide fissure-fill, cross-cutting the basement ( $38^{\circ} 45' 44.2''$  N,  $16^{\circ} 34' 11.6''$  E). (e) Field photograph of vertical fissure filled with bedded sediment, reactivating normal faults as shown by offset of veins ( $38^{\circ} 45' 34.3''$  N,  $16^{\circ} 34' 17.8''$  E). The abbreviation nml means normal. (f) Field photograph of metre wide fissure filled with bedded sediment and large boulder ( $38^{\circ} 45' 34.2''$  N,  $16^{\circ} 34' 18.0''$  E). (g) Stereographic projection showing orientations of key features and kinematic vectors. (h) Graph showing the distribution of collected fracture attribute data. (i) Orthorectified photo map extracted from photogrammetric virtual outcrop model. Orthomodel is overlain by sample windows and interpreted fracture traces and nodes for topological analysis (Sanderson and Nixon 2015). Inset gives the primary results showing ratios of I, T, X nodes and II, IC, CC branches. MES, Messinian Erosional Surface.

fills can be found at the southern end of the section by the Blu70 bar ( $38^{\circ} 45' 34.7''$  N,  $16^{\circ} 34' 18.4''$  E), where the area of the coastal platform is greatest (Fig. 2).

The microbreccia overlying the basement is exposed protruding from the concrete dancefloor of the Blu70 bar. Further up the cliff behind, transgressive marine sandstones of the San Nicola Formation are exposed in contact with the overlying Messinian limestones ( $38^{\circ} 45' 33.7''$  N,  $16^{\circ} 34' 12.7''$  E) (Fig. 2). This contact is marked by a small shale horizon thought to correspond to the Ponda Clay

Formation (Fig. 2). This outcrop lies 32 m above top-basement, suggesting a thickness of *c.* 30 m of pre-Messinian Miocene stratigraphy at the southern end of the Copanello North section.

### Copanello Centre

This small locality (50 m  $\times$  50 m) (located at  $38^{\circ} 45' 31.7''$  N,  $16^{\circ} 34' 15.7''$  E) is most significant due to the sequential fill-types

**Table 1.** Analysis of the topological results from the sample areas shown in Figure 5i

Sample information		Node analysis										Branch analysis							
Sample No.	Sample area	Total trace length	I	T	X	E	Nn	No. of lines	No. of branches	Average line length	Average branch length	Connect/line	Connect/branch	Frequency	Intensity	II	IC	CC	No. of branches
1_Copanello North	176.0	330.0	7.0	223.0	44.0	52.0	274.0	141.0	426.0	2.3	0.8	3.8	1.984	2.4	1.875	1.0	7.0	419.0	427.0
2_Copanello North	176.0	295.0	3.0	173.0	31.0	43.0	207.0	109.5	323.0	2.7	0.9	3.7	1.991	1.8	1.676	3.0	320.0	323.0	323.0
3_Copanello North	176.0	406.0	6.0	262.0	87.0	43.0	355.0	155.5	570.0	2.6	0.7	4.5	1.989	3.2	2.307	6.0	564.0	570.0	570.0
4_Copanello North	176.0	358.0	1.0	212.0	48.0	43.0	261.0	128.0	414.5	2.8	0.9	4.1	1.998	2.4	2.034	1.0	413.5	414.5	414.5
5_Copanello North	176.0	489.0	16.0	402.0	91.0	66.0	509.0	242.0	793.0	2.0	0.6	4.1	1.980	4.5	2.778	16.0	777.0	793.0	793.0
6_Copanello North	176.0	488.0	3.0	402.0	117.0	61.0	522.0	233.0	838.5	2.1	0.6	4.5	1.996	4.8	2.773	3.0	835.5	838.5	838.5
7_Copanello North	176.0	510.0	2.0	392.0	123.0	55.0	517.0	224.5	835.0	2.3	0.6	4.6	1.998	4.7	2.898	2.0	833.0	835.0	835.0
8_Copanello North	176.0	593.0	4.0	440.0	194.0	84.0	638.0	264.0	1050.0	2.2	0.6	4.8	1.996	6.0	3.369	4.0	1046.0	1050.0	1050.0
Mean_Copanello North	176.0	433.6	5.3	313.3	91.9	55.9	410.4	187.2	656.3	2.4	0.7	4.2	1.991	3.7	2.5	1.0	5.3	651.0	656.4

I, Isolated node (fracture tip); T, abutting node; X, cross-cutting node; E, where fracture intersects the sample area edge; I-I, a branch between two tips; I-C, a branch between a tip and an abutting node; C-C, a branch between two cross-cutting nodes; Nn, number of nodes. Length units are in metres; area units are metres squared.

preserved. The shallowly north-dipping base of the Messinian limestone (i.e. the MES) can be followed using breaks in the slope in the cliffs 30 m above the outcropping basement at sea-level (Fig. 2). A fault is inferred between the Copanello Centre and Copanello North outcrops to account for the *c.* 5 m vertical offset in the base-Messinian horizon (Fig. 2). Below the Messinian limestone are several metres of Miocene sedimentary rocks (conglomerates, microbreccias) exposed along road cuttings at the top of the cliffs. The exposed tonalite at the shoreline therefore lies several metres below the top-basement unconformity and represents a stratigraphically deeper section than Copanello North.

Like Copanello North, the sediment-filled fissures here have uniform north–south dilation vectors (Fig. 6a), while also displaying a wide range of orientations, with clusters developed in this section sub-parallel to reactivated vein margins. The ‘virgin’ fissures at this locality are clustered around a NW–SE orientation (Fig. 6a). The relative intensity, connectivity and aperture distributions of the fissures seen here are comparable with those seen at Copanello North, suggesting there is little change to the fracture attributes within the uppermost few metres of basement.

### Copanello South

The large NE–SW-trending shorefront locality (extending from 38° 45′ 26.0″ N, 16° 34′ 09.8″ E to 38° 45′ 30.4″ N, 16° 34′ 15.0″ E) is traversed by a small road that runs down from the top of the cliff (40 m above sea-level) to the shoreline, exposing a vertical section down through the succession (Fig. 7). The top of the road exposes the Messinian limestone and reaches the base-Messinian unconformity (the MES) at 35 m above sea-level. Here, at 38° 45′ 30.9″ N, 16° 34′ 13.6″ E, the underlying sandstone of the Miocene San Nicola Formation is <1 m thick, overlying 1–2 m of microbreccia and conglomeratic units and basement tonalite. A multi-phase half-graben structure is preserved, with NW–SE-trending normal faults (mean 121/59 SW), indicating ongoing rifting during the deposition of these units (Fig. 7a). Below and moving south from this outcrop, a *c.* 35 m vertical section of tonalitic rocks is continuously exposed down to the shore. The basement here is cut by sediment-infilled fissures, which show no significant decrease in aperture or frequency down to the shoreline. At the end of the road (38° 45′ 27.2″ N, 16° 34′ 12.5″ E), a wave-cut platform exposes a large area of basement pervasively cut by many sediment-filled fissures (Fig. 7b). This allows the basement structures to be viewed in three dimensions. Analysis of orthorectified drone images reveals the presence of a series of north–south-trending lineaments or faults and a high-strain brittle dextral shear zone defined by a band of closely spaced fault lineaments that offset the fissures (Fig. 7b).

The orientation and kinematics of the sediment-filled fissures is similar to the orientations recorded at Copanello North and Copanello Centre, with a sporadic distribution of orientations and a uniform north–south opening vector (Fig. 7e). The orientation of the subvertical ‘virgin’ fissures here are seen to cluster around ESE–WNW and NNE–SSW, and a shallowly northwards-dipping set also occurs with an east–west strike. These orientations are similar to those observed at Copanello North, but with a slight anticlockwise rotation.

At the base of the cliffs at Copanello South, sediment-filled structures occur on three scales. The largest is a single 3–15 m wide, at least 30 m high vertical fissure, trending 070°, seen both in cross-section in the cliff and in plan view in the platform (Fig. 7b–d). This fissure is dilational, with a north–south opening direction and no associated shear offset (Fig. 7c). It contains large clasts of wall rock, sediment and minor mineralization (Fig. 7d). The entrained clasts of wall rock are predominantly rounded boulders of tonalite and mafic enclaves, between which are large vuggy cavities up to 2 m in diameter (Fig. 7c). The fissure hosts calcite mineralization visible by

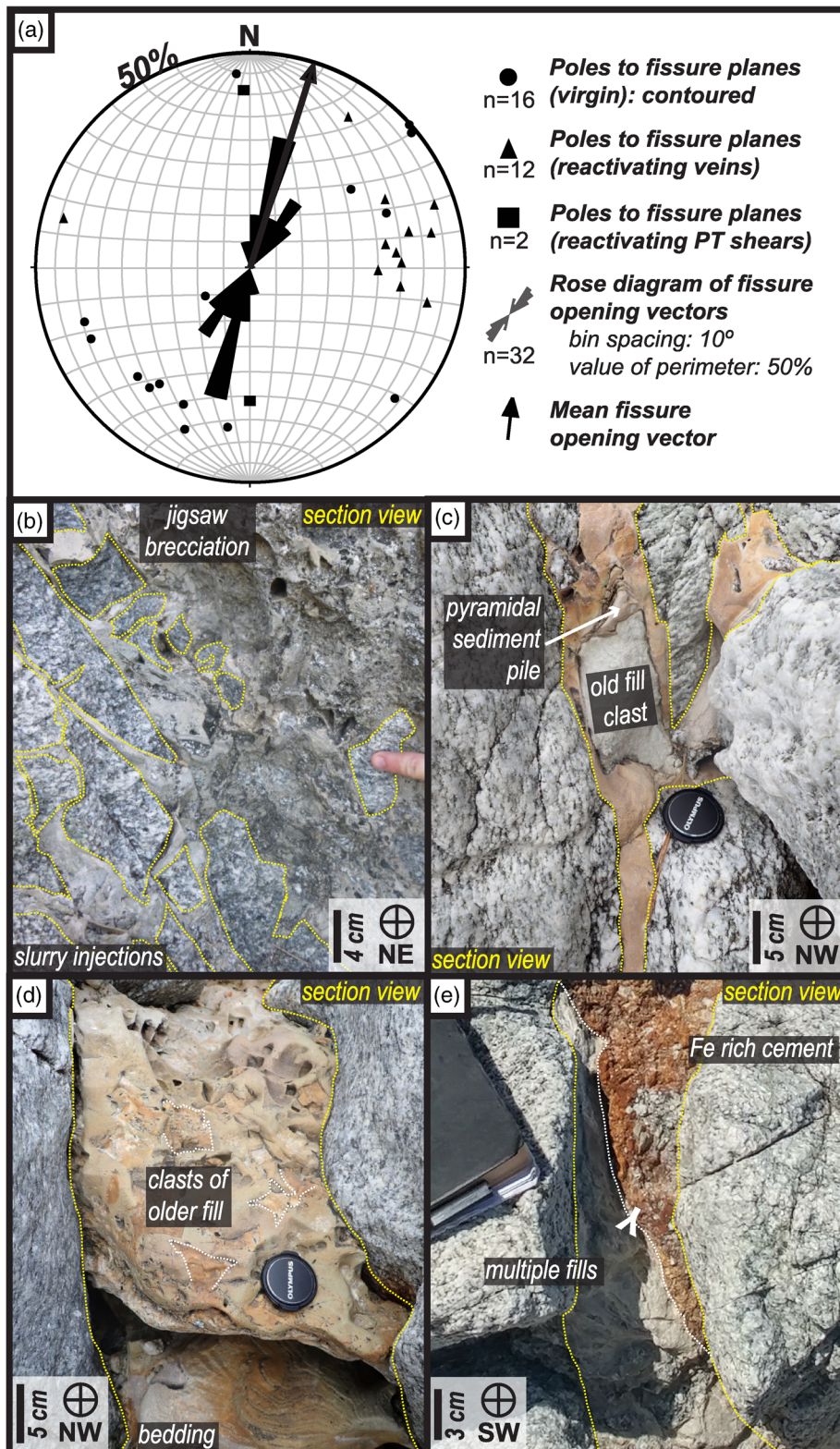


**Fig. 6.** Copanello Centre locality. Field photographs from (38° 45' 31.8" N, 16° 34' 16.1" E). (a) Stereographic projection and rose diagram showing the orientations and opening vectors of fissures. (b) Field photograph showing injection network and jigsaw breccia of sediment-filled fractures/fissures. (c) Field photograph showing multi-phase fissure-fill with clast of paler sandstone infill in a matrix of darker fine sediment. Clast is topped by pyramidal geopetal pile of sediment. (d) Field photograph of bedded and brecciated fissure-fill. (e) Field photograph of fissure containing two fills: an older paler fill and a younger Fe-stained cemented fill.

eye, which encapsulates and cements smaller clasts of breccia. Another notable characteristic is the preservation of numerous small (<2 m long) open mode I fractures in the tonalite basement up to 20 m either side of the fissure. These unfilled cracks are not connected to the top-basement palaeosurface and they appear to be strata-bound between low-angle aplite and pegmatite veins (Fig. 7c).

The wave-cut platform also hosts a large number of smaller sediment-filled fissures up to 50 cm wide. The frequency and density of these fissures is similar to those exposed at Copanello North, despite the increased formation depth (35 m below top-

basement). However, the mean aperture of the sediment-filled fissures here, excluding the large fissure, is 13 cm, which is consistent with a progressive narrowing deeper into the basement.

The smallest scale of sediment-filled cavities observed at Copanello South are millimetre-scale micro-cracks filled with a fine silt/clay-grade sediment (Fig. 7f). These branching arrays of clay-filled micro-cracks are much larger in extent (metres long rather than centimetres), denser and more widespread here than those further to the north, and, in addition, contain a more diverse infilling material. The clay-filled networks commonly consist of mutually cross-cutting

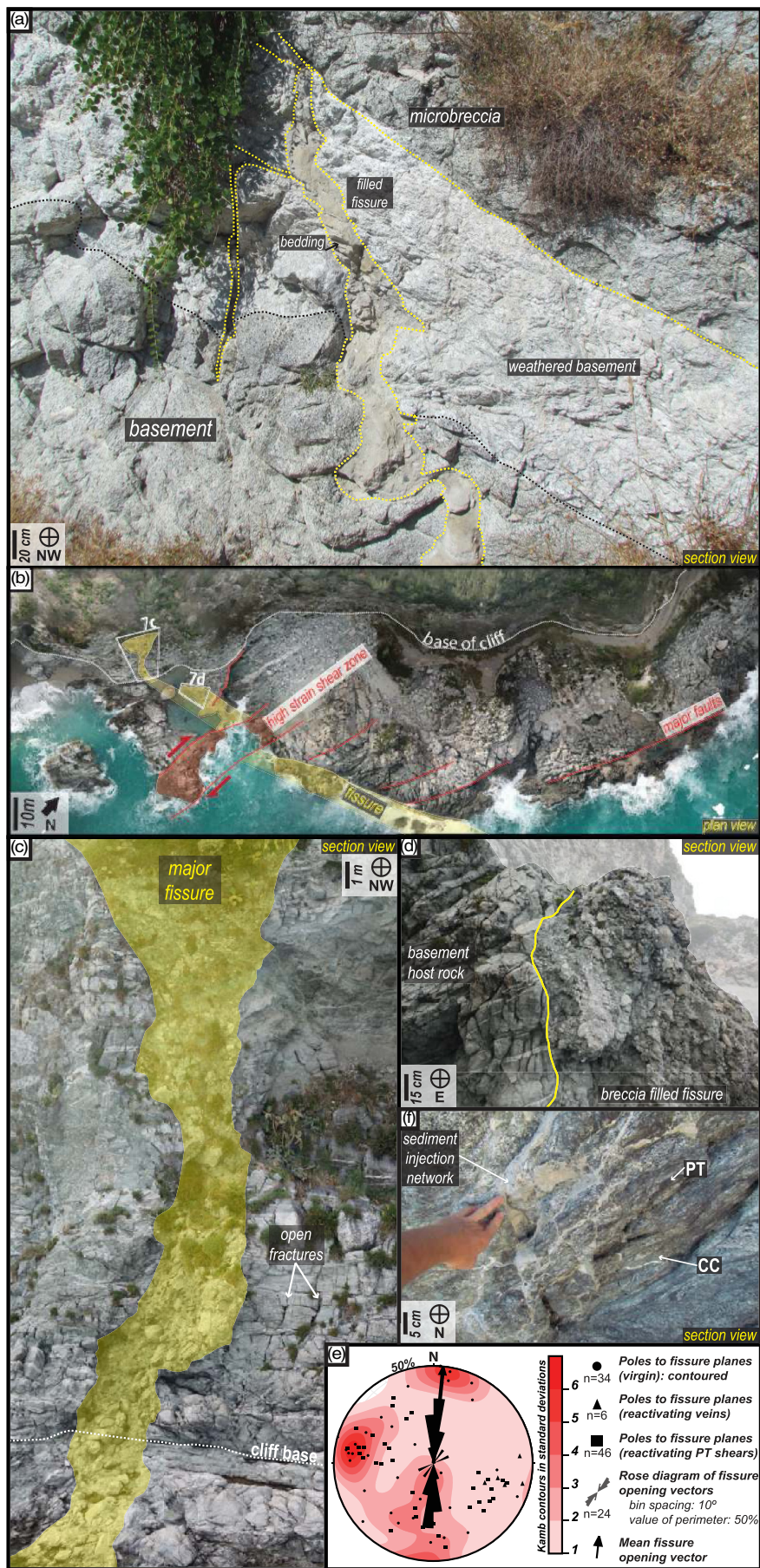


**Fig. 7.** Copanello South locality. **(a)** Field photograph of contact and cross-cutting relationships between the microbreccia, weathered basement and tonalite basement at the top of the road ( $38^{\circ} 45' 31.0''$  N,  $16^{\circ} 34' 13.7''$  E). **(b)** Orthorectified photo map extracted from photogrammetric virtual outcrop model showing major fissure (yellow) and larger faults/fault zones (red). **(c)** Orthorectified photo map of cliff section showing major multi-metre fissure (yellow) and associated damage zone of 'strata-bound' dilatant cracks. **(d)** Field photograph showing the contact between the major fissure-filled sediment and breccia and the surrounding host rock ( $38^{\circ} 45' 26.5''$  N,  $16^{\circ} 34' 10.5''$  E). **(e)** Stereographic projection showing orientations and opening directions of fissures. **(f)** Field photograph ( $38^{\circ} 45' 27.6''$  N,  $16^{\circ} 34' 10.9''$  E) showing sediment injection splay network cross-cutting pseudotachylyte and cataclasite. CC, cataclasite; PT, pseudotachylyte.

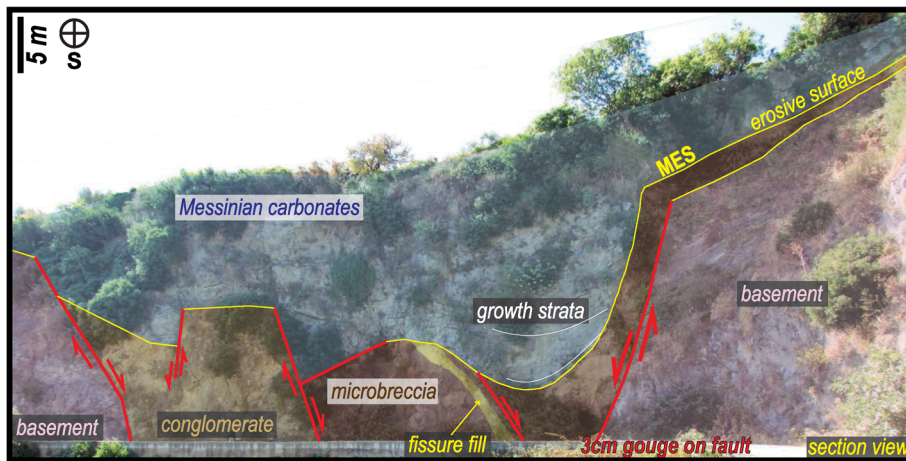


**Fig. 8.** Road-cutting locality. Field photograph showing the horst and graben multi-phase rift structures present at the road-cutting 90 m above sea-level ( $38^{\circ} 45' 23.2''$  N,  $16^{\circ} 33' 59.7''$  E). MES, Messinian Erosional Surface.

microfractures  $< 2$  mm in aperture arranged in densely packed arrays, the largest of which is 2–3 m across (Fig. 7f).

### Road-cutting

This locality lies 600 m west of Copanello Bay, 110 m above sea-level, on the Località Torrazzo, off the E90 road ( $38^{\circ} 45' 23.6''$  N,  $016^{\circ} 33' 59.1''$  E) (Fig. 2). Here, a c. 40 m high cliff around a large bend in the road exposes a small 50 m wide graben, with fault-bounded units made up of tonalitic basement, conglomerate and microbreccia of the San Nicola Formation, and the graben filled with overlying Messinian limestones (Fig. 8).

The normal faults strike NNW–SSE ( $150$ – $170^{\circ}$ ) and dip  $65$ – $75^{\circ}$  east or west. These faults host a pale, well-cemented fine-grained fault gouge ( $< 5$  cm thick) with fault-parallel foliations and slickenlines that show sinistral-normal, oblique-slip fault displacements (itches of  $50$ – $85^{\circ}$ ). These normal faults offset the tonalite, conglomerate and microbreccia, with lateral thickening preserved in

the microbreccia unit on the western side of the graben (Fig. 8). This is consistent with growth faulting during the deposition of the Miocene coarse-grained units. The overlying carbonates also show clear growth strata in the graben (Fig. 8). This later phase of extensional faulting may be broadly correlative with the larger faults observed at Copanello North that cut the Messinian strata. Bedding within the matrix sediment in the conglomerate and breccia is sub-horizontal, indicating that limited rotation of the fault blocks has occurred subsequent to deposition.

Cutting the central horst block of microbreccia is a large, sediment-filled fissure (c. 50 cm in aperture) trending  $170/65$  W, which is itself truncated by the overlying MES and Messinian carbonates (Fig. 8). The sedimentary fill of the fissure appears to be identical to fills seen at the Copanello and Pietragrande coastal outcrops. Notably missing from this section are the units from sandstones of the San Nicola Formation and the Ponda Clay Formation (Fig. 8). These units are often absent in the marginal sectors of the Crotona Basin, where the Messinian carbonates are

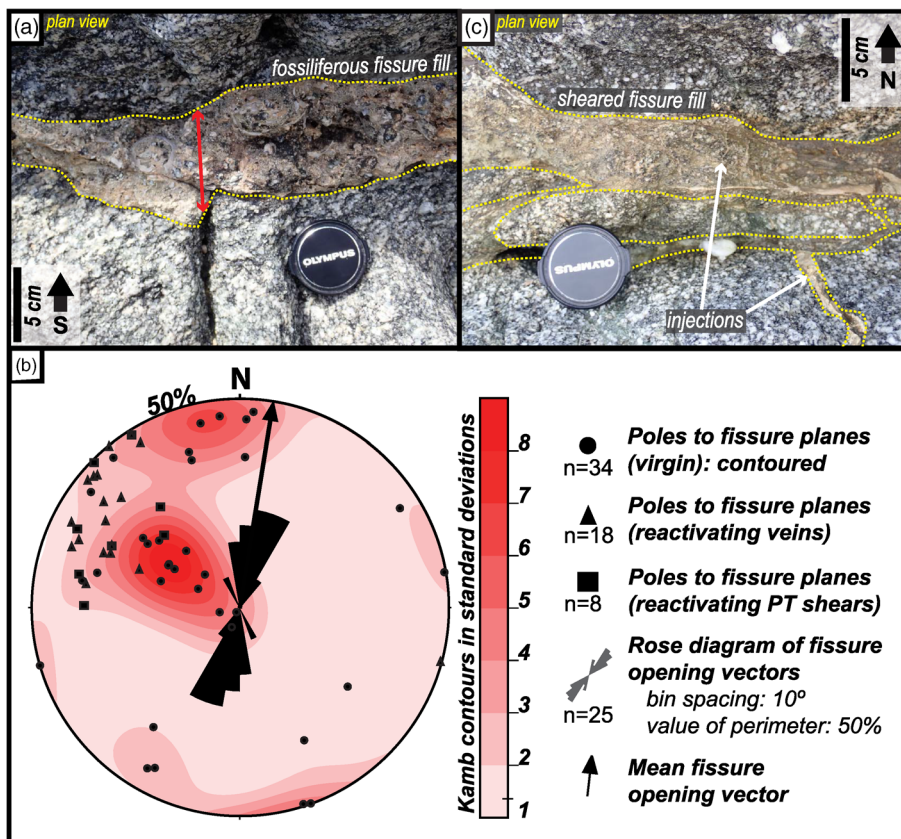


**Fig. 9.** Pietragrande locality. (a) Field photograph of fissure filled with fossiliferous sediment and breccia ( $38^{\circ} 45' 11.8''$  N,  $16^{\circ} 34' 06.6''$  E). (b) Stereographic projection showing orientations and opening directions of fissures. (c) Field photograph of sheared fissure-fill and micro-injection network ( $38^{\circ} 45' 11.8''$  N,  $16^{\circ} 34' 06.6''$  E).

seen to rest on the coarse-grained deposits of the San Nicola Formation with a local low-angle unconformity (Massari *et al.* 2010). This may be the result of local topographic variation and sediment pathways during the late Miocene, which may have prevented the deposition of these formations.

### Pietragrande

The Pietragrande locality is situated 800 m south of Copanello Bay on the Torrazzo headland ( $38^{\circ} 45' 11.8''$  N,  $16^{\circ} 34' 06.6''$  E), c. 2.5 km from the Catanzaro Fault (Fig. 2). It is not clear from existing outcrops exactly where the base-Messinian or top-basement contacts lie in relation to the basement exposed here. However, tracing the base of the Messinian carbonates using breaks in the

slope suggests that the base-Messinian unconformity (the MES) is c. 50 m above sea-level at Pietragrande.

The sediment-filled fissures outcropping here show a similar range of orientations and uniform north–south dilation vectors, as seen at other localities (Fig. 9b), but with smaller numbers of more concentrated clusters. The ‘virgin’ fissures at Pietragrande occur in two main subvertical clusters oriented broadly ENE–WSW and NE–SW. This concentration of fissure orientations, compared with Copanello, may reflect a consolidation and alignment of fissures with increased depth into the basement. In addition, the fissure apertures are much narrower than elsewhere (mean 2.7 cm) and many are associated with small zones of mutually cross-cutting microfractures (Fig. 9c) not observed at other localities. They consist of numerous densely packed bifurcating and linking filled

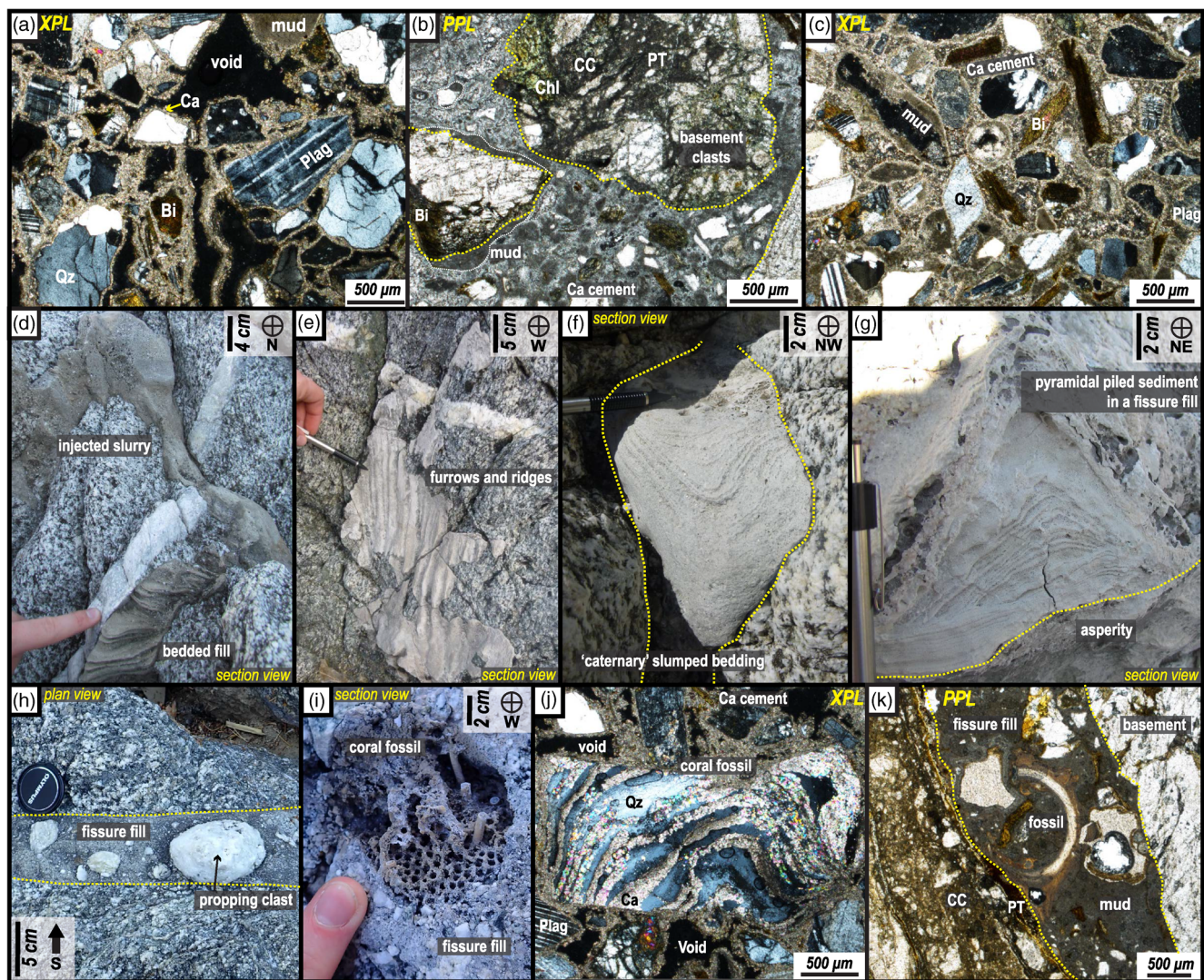


**Fig. 10.** Figure summarizing the breccias, sediments and sedimentary structures present within fissure-fills across Copanello. (a) Thin section photomicrograph showing fissure-fills sandstone petrology consisting of angular grains of quartz, plagioclase and biotite surrounded by calcite cement in an isopachous to cockade texture. (b) Thin section photomicrograph of breccia showing millimetre-sized clasts of basement in a matrix of angular grains in a carbonate mud and calcite cement. Clasts feature chloritized biotite, cataclasite and pseudotachylyte. (c) Thin section photomicrograph of fissure-fill showing angular grains of basement material surrounded by carbonate mud and cemented by cockade/isopachous calcite. (d) Field photograph of bedded and injected fissure-filling sediment cross-cutting a vein ( $38^{\circ} 45' 34.1''$  N,  $16^{\circ} 34' 17.4''$  E). (e) Field photograph of sediment plastered on fissure wall and hosting furrows and ridges ( $38^{\circ} 45' 34.1''$  N,  $16^{\circ} 34' 17.4''$  E). (f) Field photograph of bedded fissure-fill with slumped ‘catenary’ bedding ( $38^{\circ} 45' 34.2''$  N,  $16^{\circ} 34' 18.0''$  E). (g) Field photograph showing geopetal sediment piled on an asperity ( $38^{\circ} 45' 34.3''$  N,  $16^{\circ} 34' 18.7''$  E). (h) Field photograph of fissure filled with sediment and rounded breccia clasts that act as a proppant ( $38^{\circ} 45' 37.5''$  N,  $16^{\circ} 34' 15.7''$  E). Clasts are rounded from rolling at the palaeosurface prior to falling into fissure. (i) Field photograph of fissure-fill containing fossilized coral growths ( $38^{\circ} 45' 34.3''$  N,  $16^{\circ} 34' 17.9''$  E). (j) Thin section photomicrograph of mineralized fossil fragments from a fissure-fill. Fossil is remineralized in quartz and calcite. (k) Thin section photomicrograph of a mud-rich fissure-fill containing a bivalve fossil. Fissure cross-cuts basement, cataclasite and pseudotachylyte. Bi, biotite; Ca, calcite; Chl, chloritized biotite; CC, cataclasite; Plg, plagioclase; PT, pseudotachylyte; Qz, quartz.

microfractures, each with an aperture <0.5 cm, arranged in a sub-parallel corridor up to 20 cm wide.

## Infills and microstructures

### *Copanello–Pietragrande*

The vast majority (>80%) of the sedimentary fills in the Copanello area are hard, pale, medium- to coarse-grained sandstones, often with variably sized breccia clasts, and occasional fossils (Figs 5a–f, 6b–e, 7b–d, f, 9a, c). The sandstones preserve sedimentary structures, but these are not ubiquitous because many fills consist of simple, massive, well-sorted sandstones and conglomerates/breccias. In outcrop, the grain size distribution appears uniform within most individual fissures, but it appears to vary significantly between fissures. For the majority (>80%), the grain sizes are between 200 and 500 µm. In outcrop, the sandstones are well cemented, although no widespread carbonate mineralization is observed, except in the large fissure at Copanello South.

In thin section, the sand grains are shown to primarily consist of angular to subangular grains of quartz, biotite and feldspar (Fig. 10a). In addition to monomineralic grains, there are fragments of tonalite, aplite vein, pseudotachylyte, fossils, cataclasite and chloritized biotite (Fig. 10b). Surrounding the sandstone grains are small volumes of calcite cement and a fine carbonate mud (Fig. 10c). The carbonate mud occurs both directly against the grain surface (i.e. under the calcite cement; Fig. 10c) and in intergranular cavities (Fig. 10b), indicating that the precipitation of calcite and the accumulation of carbonate mud were contemporaneous. Some fills show a complete absence of interstitial muddy material and therefore the calcite rind growth continues into the adjacent open pore spaces.

Despite the hard, cohesive nature of the sandstone in the field, in thin section the grains appear largely uncompacted, with large volumes of highly interconnected intergranular pore space between unaligned grains (Fig. 10a–c); visual estimates in thin section suggest a primary porosity of *c.* 15–25%. This pore space is sometimes occluded by carbonate mud or calcite cement (Fig. 10b). The lack of compaction is thought to be caused by the host tonalite acting as a mechanical proppant, preventing the weight of overbearing sediments from dewatering and compacting the fissure-fill sediment.

The angularity and composition of the clasts suggest a local tonalitic basement origin, which is consistent with the frequent presence of clasts of pseudotachylyte and cataclasite. The occurrence of calcareous muds and marine fossils within the fissures (Figs 9a, 10i–k) suggests that the fills are sourced from a marine palaeoenvironment (Dowey *et al.* 2017). Coatings of calcareous mud (Fig. 10c) may indicate that the sediment grains were rolled along the seafloor, collecting mud prior to deposition in the fissure.

Where bedding is observed within the fissures of Copanello and Pietragrande, it is typically defined by thin silt laminations and sharp variations in grain size between normally graded beds (Fig. 10d). The bedding planes are commonly horizontal, demonstrating that these fissures have not experienced significant rotation following their formation. Where the bedding is not horizontal, it is typically fissure-parallel and appears to reflect a ‘plastering’ effect of sediment emplaced against the rough surface of a fissure wall (Fig. 10e). Where this plastering process has occurred, steeply inclined branching furrows and ridges are locally preserved in finer sediment fills, trending parallel to the fissure wall (Fig. 10e). These corrugated sedimentary structures are formed in low-energy environments, such as karst systems, where gravity-driven fluids deposit and shape the suspended fine-grained sediments (Flood 1981). Unlike ripples, furrows and ridges of this kind are formed trending parallel to the principal fluid flow direction and tend to

converge and simplify with depth (Fig. 10e). In the larger sandstone-filled fissures, bedding is locally observed to have been deformed (Fig. 10f). This deformation consists of a localized slumping or drooping of bedding surfaces to create a markedly catenary U-shaped curve (Fig. 10f). These structures are interpreted to have formed in unconsolidated sediment where accommodation space beneath the fill became available and the still-soft sediment subsided further into the cavity below.

Further evidence for gravity-driven fluid and sediment transport comes from the preservation of pyramidal accumulations of sandstone within large vertical fissure-fills (Fig. 10g). These geopetal ‘piles’ of sediment occur directly overlying any sub-horizontal planar surface within a fault cavity, such as entrained clasts and fault wall asperities. The piles vary in size from a few millimetres to tens of centimetres across and, where exposed in cross-section, show a gradual steepening of bedding sets upwards and towards the margins (Fig. 10g). This feature is typical of geopetal accumulations of sediments that have been washed into open cavities (e.g. Wright *et al.* 2009; Woodcock *et al.* 2014; Hardman *et al.* 2020).

Entrained clasts of tonalitic basement are abundant in many basement-hosted fissures around Copanello and Pietragrande (Fig. 10h). These clasts vary significantly in diameter from centimetres to multiple metres, often in broad correlation with the aperture size and palaeosurface proximity of the hosting fissure. The breccia clasts consist of both well-rounded and angular blocks (Fig. 10h). Most breccia fills are chaotically oriented, rounded boulders (up to several metres in diameter) of basement material, which are typically found within larger fissures and those closest to the top-basement unconformity (Fig. 10h). These rounded clasts may be overlain by bedded sediment and held within a sediment matrix, suggesting that their emplacement within the fissure cavity predates, or is coeval with, the emplacement of the sediment. Other commonly occurring styles of brecciation within the fissures include locally developed jigsaw-type breccias, which form where clast fragments of wall rock are seen only slightly displaced from their original position, and are held in position by the sandstone matrix (Woodcock *et al.* 2014; Hardman *et al.* 2020). The sediment-filled fissures at Copanello Centre also host re-brecciated fills, whereby clasts of semi-lithified sediments are brecciated within a matrix of younger sedimentary material (Fig. 6c, d). The cross-cutting relationships observed here indicate a relative age relationship for the different sediment accumulations, ending with a markedly iron-stained unit (Fig. 6e). Overall, however, the fissures are interpreted to have been emplaced broadly contemporaneously.

Fossiliferous material is observed within fissure-fills throughout Copanello and Pietragrande, both in outcrop and in thin section (Fig. 10i–k). Like the breccia clasts, the fossil fragments vary in size depending on the aperture of the hosting fissure and the depth below top-basement, with larger more complete assemblages observed closer to the unconformity (Fig. 10i). The fossils typically consist of fractured corals (Fig. 10j) and bivalves (Fig. 10k). Although the majority of fossils observed show clear evidence of transport prior to deposition (e.g. fracturing or rotation), some coral growths at Copanello North are potentially autochthonous because they are largely unfractured, unrotated and are situated on the top or sides of large clasts (>1 m) wedged within fissure cavities close to the top-basement erosion surface.

Less common arrays of finer, branching sediment fills display fracture-parallel foliations within the enclosed sediments (Fig. 6b). These branching fractures occur as micro-scale fractures (<1 mm in aperture) filled with clay and fine silt and also as larger meso-scale fractures (<10 cm in aperture) filled with chaotic sediment breccia matrix. These fractures tend to originate from large, often bedded, fissure-fills, but show splaying and branching fault architectures, which rapidly narrow toward the tips (Fig. 6b). The

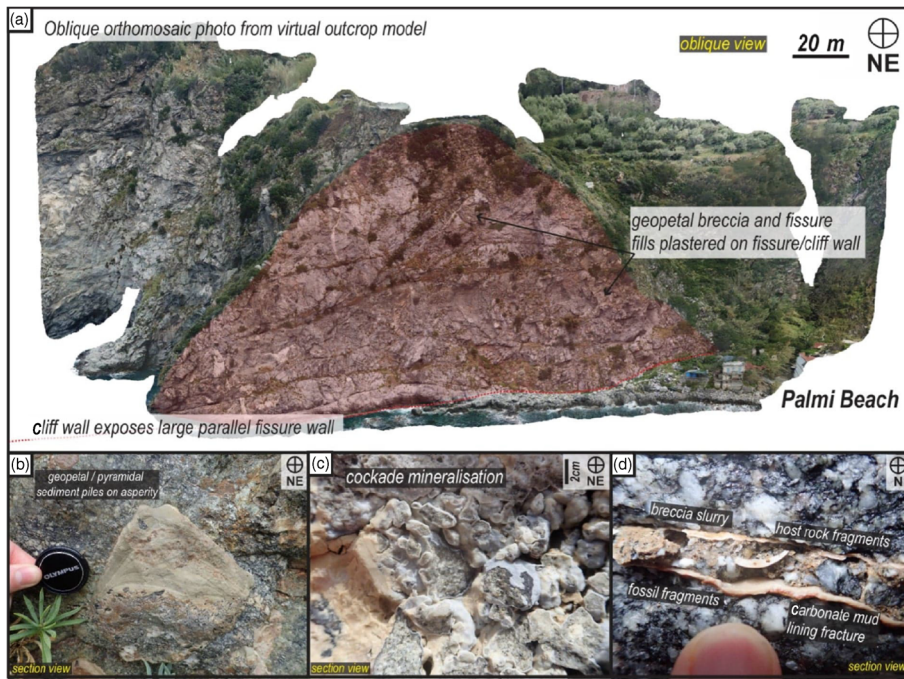


**Fig. 11.** Figure summarizing the geological relationships of fissures at Palmi. (a) Oblique orthomosaic image from virtual outcrop model highlighting the profile of a large fissure in the cliff wall. (b) Field photograph of a geopetal sediment accumulation on an asperity within a fissure cavity. (c) Field photograph of cockade style mineralization texture of breccia clasts within a fissure. (d) Field photograph of injected fissure with a carbonate mud lining the fault cavity encapsulating a chaotic slurry of breccia and fossil fragments.

chaotic fills are a poorly sorted matrix of sediment and breccia clasts, which occasionally show asymmetrical laminations along the fracture walls. Where these fractures narrow through bifurcation or tipping-out, the entrained sediment becomes finer and may be indicative of an injected ‘slurry’ of material. The microfractures consist of a homogenous, pale silt- to clay-grade micritic material that forms dense branching networks of fractures. These fractures do not appear to cross-cut one another, instead forming abutting and splay intersections, suggesting that they formed coevally. The clay-splay networks are seen to locally cut older fissures and originate from larger fissures (e.g. Fig. 9c). The microfractures plausibly formed due to hydraulic overpressure and injection within a single instantaneous event. The increased prevalence and magnitude of injections of all types towards Copanello South may be associated with proximity to the major east–west fissure at this location and/or to the increased depth of the fissures within the basement.

### Palmi

According to Montecat *et al.* (1991), sediment-filled fissures with vertical dimensions of up to at least 10 m and apertures of up to tens of centimetres are widely associated with fault scarps close to the Straits of Messina adjacent to Scilla in SW Calabria. Some of the best examples are found cutting late Carboniferous basement tonalites of the Aspromonte Massif in the coastal exposures around Palmi (Figs 1a, 11).

The cliff and coastal platform here preserve large sediment- and collapse breccia-filled fissures >150 m deep and several hundred metres in lateral extent (Fig. 11a). The fissure apertures are 1.5–10 m and are pervasively infilled by sediment, conglomeratic boulders and breccia clasts derived from the surrounding basement rocks. Rind-like calcite mineralization textures are more widespread than at Copanello–Pietragrande. Geopetal sediment fills and other way-up criteria indicate that the locally bedded sediments were passively deposited in the cavities from above (Fig. 11b, c).

At the base of the cliffs and elsewhere along the shore section, large numbers of branching, fine-grained narrow fractures (<3 cm) are observed, lined by fine-grained mud at the contact with the wall rock, with cores of chaotic breccia slurry (Fig. 11d). These

structures appear more typical of injection fabrics, suggesting that these represent the local hydraulic injection of sediment into wall rock during or immediately following emplacement.

## Discussion

### Early structural history

Caggianelli *et al.* (2005) have suggested that the pseudotachylytes and associated cataclasites in the southern part of the Copanello and Pietragrande areas are related to shallowly ESE- or east-dipping normal fault zones. These observations are consistent with our findings. Using optical microscopy and scanning electron microscopy, Caggianelli *et al.* (2005) described spherulitic and foliated microlites of plagioclase and biotite in the pseudotachylyte matrix and, through thermobarometry and available geochronological data from the region, suggested that the seismogenic events occurred in the time period 30–21 Ma at a depth of *c.* 10 km. This Oligo-Miocene age is consistent with the timing of rapid exhumation and extensional faulting in the region (Thomson 1994; Van Dijk *et al.* 2000), but precedes the mid-Miocene Tortonian–Messinian opening of the Catanzaro and Siderno graben (Caggianelli *et al.* 2000; Langone *et al.* 2014).

A palaeostress inversion analysis was undertaken on the cataclasite- and pseudotachylyte-bearing faults where slickenlines are preserved ( $n = 36$ ; Fig. 12a, b). The resolved  $\sigma_1$  axis lies close to subvertical (81/018), whereas the  $\sigma_3$  axis has a near-horizontal orientation (04/262) (Fig. 12c, d). The results are consistent with a normal faulting regime (stress ratio  $R = 0.41$ ) with an east–west direction of tectonic extension and is in good agreement with the previous findings of Caggianelli *et al.* (2005).

### Fissuring: age and significance

Our observations indicate that the fracture-hosted cavities in the tonalitic basement and early cover units in this region of Calabria are extensional or transtensional fault-related fissures formed at, or close to, the palaeosurface (Fig. 13a). They formed subsequent to the regional erosion and exhumation of the basement in the Oligocene–Miocene (Thomson 1994; Rossetti *et al.* 2004). Erosion of the Calabria basement sourced the deposition of thick Oligo-

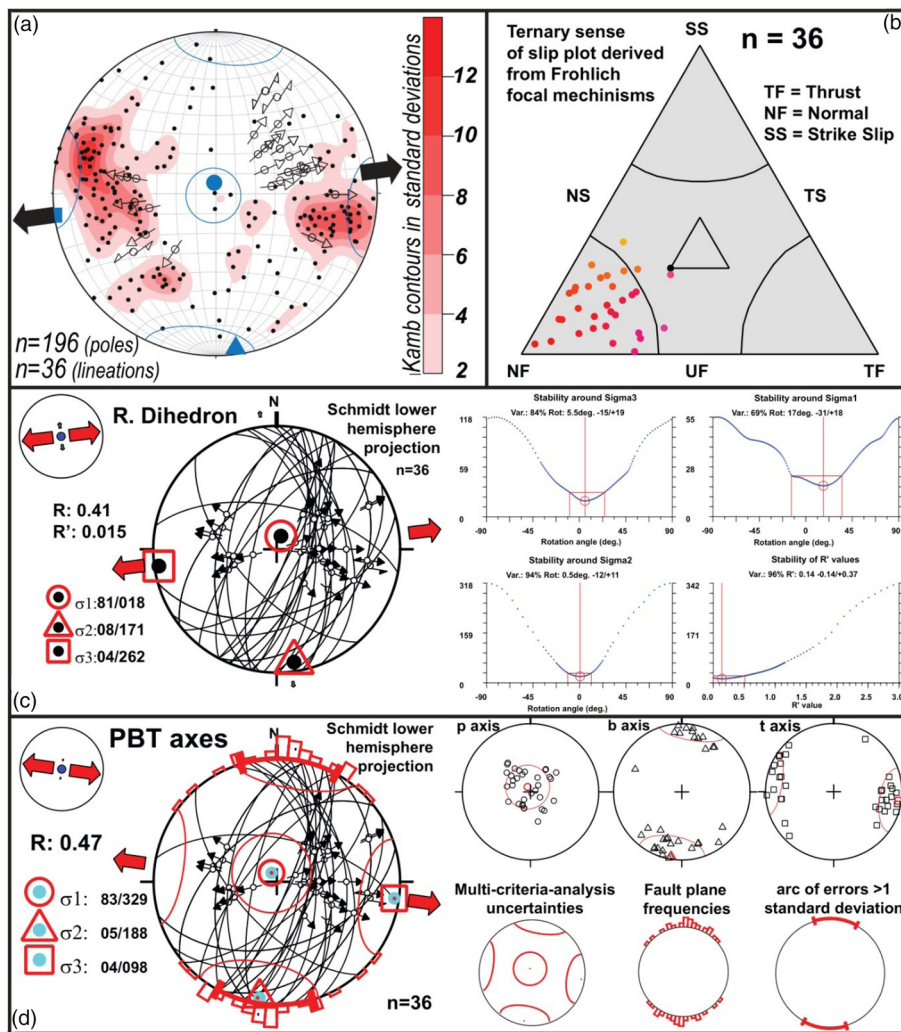


**Fig. 12.** Summary of the palaeostress inversion for the cataclasite and pseudotachylyte hosting faults. (a) Stereographic projection of the data used for the palaeostress inversion with fault vector lineation data shown with arrows and poles to fault planes as contoured dots. (b) Ternary plot showing the fissure systems in fractured basement distribution of slip senses from resolved focal mechanisms, with grouping of data around normal faults. NS, transtension; TS, transpression; and UF, undefined. (c) Summary results of palaeostress inversion using improved right dihedral method of [Angelier and Mechler \(1977\)](#) and [Delvaux and Sperner \(2003\)](#). Left: resolved stereographic projection with stress axes. Right: stability profiles around stress axes showing margin from the collected vector data. (d) Summary of results from palaeostress analysis using PBT axes method. Left: resolved stereographic projection with stress axes and uncertainties. Right: resolved contraction (p), neutral (b) and extension (t) axes and summary of different uncertainties using multi-criteria analysis, fault plane orientation frequencies and standard deviations.

Miocene flysch units in the southern sectors of the Calabrian arc (the Stilo-Capo D'Orlando Flysch; [Cavazza et al. 1997](#)) outside the study area. During the mid- to late Miocene, the remaining exposed basement was widely overlain by siliciclastic sediments associated with the development of a regional non-conformity (the main erosional unconformity of the present study). The clastic material was mostly deposited by flowing water currents and/or due to gravity into a network of long-lived open submarine cavities ([Fig. 13b, c](#)).

In thin section, the sandstones within the fissures ([Fig. 10a–c, j, k](#)) and the matrix sandstone of the overlying conglomerates and microbreccias ([Fig. 2c, d](#)) appear identical, with similar clast mineralogy, calcite cements, calcareous muds and fossil materials. This suggests that the sediments in both the cover sequences and the underlying fissure-fills are derived from the same local basement source rocks. Cross-cutting relationships with the filled fissures show that they formed immediately prior to, or during the deposition of, the overlying conglomerate, representing the base of the San Nicola Formation, and probably ceased forming following the deposition of the microbreccia unit because we observed fissures cross-cutting and being stratigraphically cut by only the microbreccia and the conglomerate cover units ([Fig. 13c](#)). The sandstones in the upper part of the San Nicola Formation are almost identical in composition to those forming the matrix of the fissure-fills, the microbreccia and the conglomerate, and also contain very similar fossiliferous material ([Massari et al. 2010](#); [Massari and Prosser 2013](#); [Siddoway et al. 2019](#)). This suggests that the fissure-fill sands are marine and most likely late Serravalian–early Tortonian (*c.* 11 Ma) and that they predate the

formation of the erosional unconformity that forms the base of the overlying (non-fossiliferous) Messinian sequence (i.e. the MES). This means that in those areas where the Messinian carbonates lie directly on the basement, the fissures effectively preserve a 'missing' stratigraphic record of the older Miocene sedimentary material ([Fig. 13d](#)).

Given the uniform north–south opening vectors of fissures across the whole study area ([Figs 5g, 6a, 7e and 9b](#)), it is likely that the fissures are tectonic in origin. Given the age constraints provided by the fissure-fills, and the proximity to the Catanzaro Fault, we propose that the fissures formed during Miocene sinistral transtension associated with the development of the Catanzaro graben ([Fig. 1a, d](#)) ([Van Dijk et al. 2000](#); [Spina et al. 2011](#)). This Miocene rifting is a recognized phase of extension/transtension associated with the back-arc Tyrrhenian extension ([Figs 1d and 2](#); [Ghissetti and Vezzani 1981](#); [Monaco et al. 1996](#); [Spina et al. 2011](#); [Brutto et al. 2016](#)).

#### **Fissure-filling processes: injection v. passive sedimentation**

Sediment-filled fracture bodies are widely referred to in the literature as either 'neptunian dykes' or 'injectites' (e.g. [Richter 1966](#); [Siddoway and Gehrels 2014](#)) and are typically diagnosed by the lack of internal sedimentary structures ([Jonk 2010](#); [Hurst et al. 2011](#)). Injectites are generated where overpressure develops in a poorly consolidated, uncemented sandstone, leading to hydraulic fracturing in an adjacent (usually, but not exclusively) overlying lithology (e.g. [Jonk et al. 2003](#); [Hurst et al. 2011](#)). A previous study of the sediment-filled fissures of the Copanello and Pietragrande

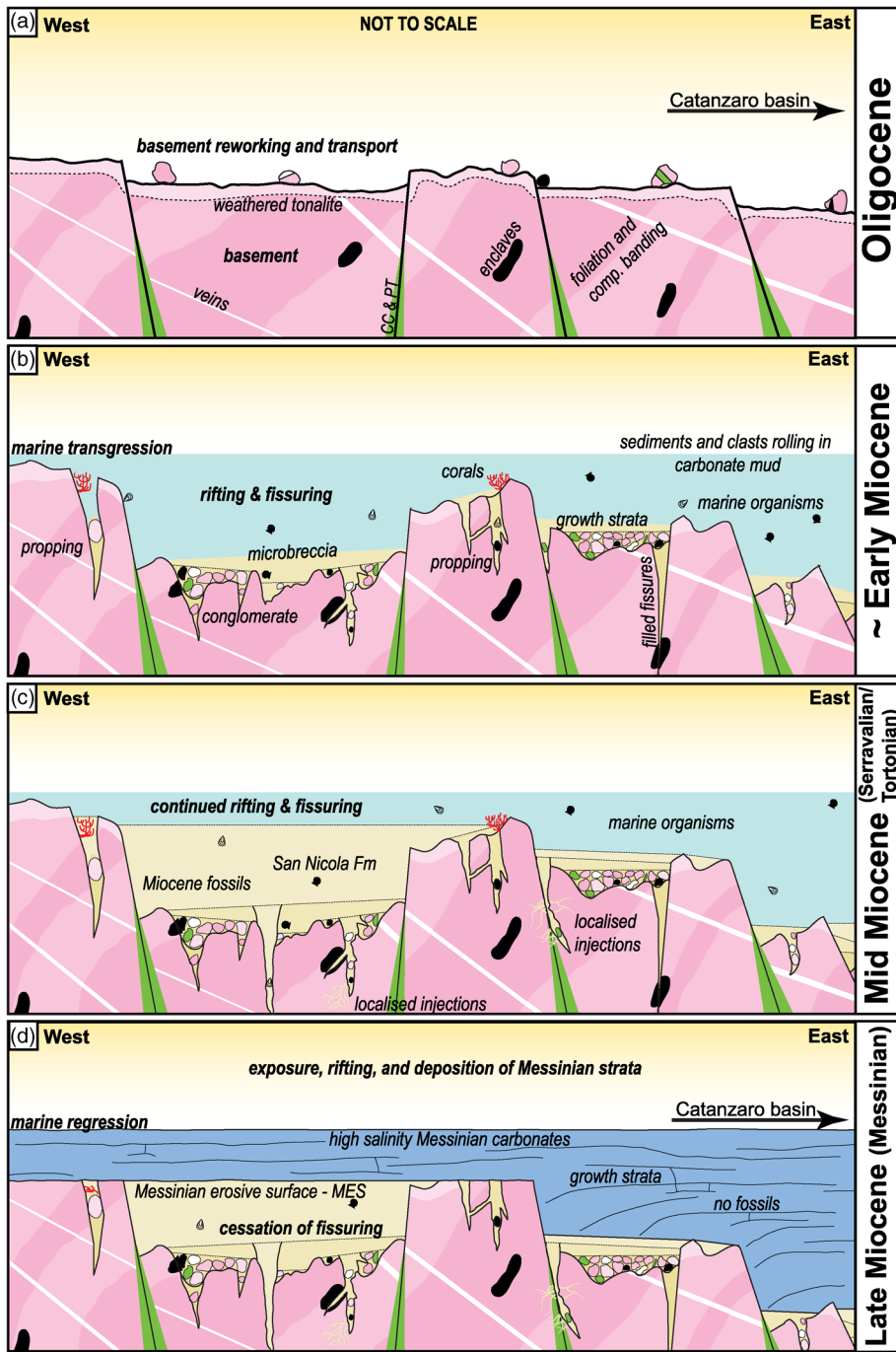


Fig. 13. (a–d) Figure summarizing the geological model for the formation and evolution of fissures at Copanello. See text for further details. CC, cataclastite; PT, pseudotachylyte.

area has referred to these fills as mostly injectites (Siddoway *et al.* 2019). Given the overwhelming evidence presented here for gravity-driven and/or water-lain deposition of the sediment and clast fills, it is suggested that sediment-filled fracture bodies occurring in the study area would be better described as fissure-fills. In this regard, they share many similarities with the sediment-filled fractures described in sub-unconformity fractured basement rocks (e.g. Holdsworth *et al.* 2019, 2020; Ceccato *et al.* 2021) and carbonates (e.g. Hardman *et al.* 2020).

Although gravity-driven and water-lain sediment influx is proposed as the primary filling mechanism for the studied fractures, a minority of examples do show evidence consistent with hydraulic injection. These sediment slurry and clay fills typically originate from nearby, wider aperture bedded fissures, suggesting that highly localized changes in fluid pressure can occur within the network, driving localized injection according to the mechanisms suggested by Palladino *et al.* (2018, 2021). Given

that these fissures probably formed as a result of ongoing Miocene rifting, it is not unreasonable to suggest that new dilatant fractures, or jogs, could form after other fissures had been opened and filled. If these dilatant voids were to develop abutting a fissure filled with unconsolidated sediment, then the differential pressure associated with the rapid generation of a new void space could rapidly draw-in any loose material or fluids (Hardman *et al.* 2020). In addition, any sudden changes in void geometry or volume as a result of ongoing tectonic deformation could create significant local overpressures within the trapped sediment fills, resulting in local injection episodes. These tectonically driven mechanisms could also explain the increased prevalence of injected material with depth below the palaeosurface and proximity to tectonic fissures at Copanello South and Palmi. Previous researchers have demonstrated and discussed the link between seismicity and the collapse of fault voids in the subsurface (e.g. Sibson 1994; Holdsworth *et al.* 2019). Given the evidence for seismicity from the Oligocene to the

present day across Calabria (e.g. Monaco *et al.* 1996; Caggianelli *et al.* 2005; Cirrincione *et al.* 2015; Tripodi *et al.* 2018), it is highly likely that seismic activity could lead to the local injection and remobilization of the fissure-filling material deeper in the basement prior to lithification.

### **Mineral cements and textures**

Visible mineralization and mineral veining are fairly sparse within the fissures at Copanello and Pietragrande, although they are more widespread at Palmi. Rind-like grain-coatings of calcite partially cement the sedimentary material both within the fissures and the overlying Miocene cover sequences. This calcite typically consists of small (<5 µm) sparry crystals that grow syntaxially into the available void spaces (e.g. Fig. 10a). This syntaxial crystal growth occurs from the fracture walls inwards, or from clasts/grains outwards, and is indicative of ‘cavity-filling’ mineralization that occurred after the voids had developed (e.g. Cox and Etheridge 1983). These features show some similarity with the cockade textures described by Frenzel and Woodcock (2014) and Cox and Munroe (2016). Irrespective of whether or not they represent true cockade textures, they certainly indicate that sustained fluid flow leading to mineralization has occurred through the highly porous and permeable fissure-fill systems.

### **Comparison with other fractured basement reservoirs**

Sub-unconformity fractured basement reservoirs are known to be associated with economically significant accumulations of groundwater (e.g. the ‘hard rock aquifers’ of Lachassagne *et al.* 2021), hydrocarbons (e.g. Gutmanis 2009; Trice *et al.* 2019) and geothermal fluids (e.g. Vidal and Genter 2018). Hydrocarbon plays most typically involve the development of a basement trap formed from a palaeohigh, known informally as a ‘buried hill’ (e.g. Biddle and Wielchowsky 1994). In the majority of cases, such a high forms in the uplifted footwall of rift-related normal faults and is similar to the setting of the basement-hosted fissure systems in Calabria (Montenat *et al.* 1991).

The uplifted basement high is typically capped by a local- to regional-scale erosional unconformity, meaning that the top-basement rocks experience a period (or periods) of subaerial exposure at the surface. This can lead to weathering and saprolite development, forming a carapace of arenaceous material with enhanced intergranular porosity. This is well documented in hard rock aquifers located in continental cratons (see Lachassagne *et al.* 2021) and hydrocarbon-related basement reservoirs, such as the Utsira High in the Central North Sea (e.g. Riber *et al.* 2015) and proposed onshore analogues (e.g. Riber *et al.* 2017; Ceccato *et al.* 2021). Typically, diagenetic processes have broken down the more unstable ferromagnesian minerals (e.g. amphibole and pyroxene) and feldspars in the basement rocks into clay, leading to the creation of secondary porosity and further fracturing due to volume changes and void collapse (Riber *et al.* 2017). Although there is limited evidence of weathering of the basement in the Calabrian examples, it appears to have been relatively minor in the present study area, although deep weathering of the basement has been recorded elsewhere in Calabria (e.g. Le Pera and Sorriso-Valvo 2000).

The near-surface setting is known to have a very significant influence on fracture development in strong basement rocks. Recent studies have documented the development of massively dilatant near-surface fault and fracture systems in subaerial zones of active rifting (e.g. van Gent *et al.* 2010; von Hagke *et al.* 2019; Weismüller *et al.* 2019). The normal faults reach the surface as wide tensile fissures with well-connected and deeply penetrating void spaces that extend to depths of many hundreds of metres (Holland *et al.* 2011; van Gent *et al.* 2010). These subterranean cave systems are

inevitably prone to partial filling with wall rock collapse breccia and water-lain sediments from above and by the deposition of near-surface hydrothermal mineral deposits originating at depth. They can also allow subaerial weathering processes to extend down to greater depths into the basement (e.g. Ceccato *et al.* 2021).

Sediment- and mineral-filled fissures very similar to those seen in Calabria have been described in subsurface fractured basement reservoirs, such as those from the Clair (Holdsworth *et al.* 2019) and Lancaster (Holdsworth *et al.* 2020) hydrocarbon reservoirs along the Rona Ridge offshore NW Scotland. Sidewall cores from the subsurface basement in this region show that these rocks are cut by networks of naturally propped fissures that extend hundreds of metres below the local erosional, top-basement unconformity. Weathering profiles are also relatively localized and limited in the Rona Ridge examples. The main difference is that the Clair and Lancaster examples appear to be associated with much more extensive near-surface hydrothermal mineralization than Calabria. Nevertheless, the overall similarity suggests that the surface outcrops seen in southern Italy represent a plausible surface analogue example of this type of sub-unconformity reservoir where the effects of weathering are relatively limited.

### **Conclusions**

The Miocene age network of sediment-filled fractures cutting Carboniferous crystalline basement in the Copanello–Pietragrande area of southern Italy was mostly formed due to gravity- and water-lain-filling of open fissures in a sub-unconformity geological setting. The highly porous (locally up to 25%), mainly medium- to coarse-grained carbonate-cemented breccias and sandstones are essentially continuous with the overlying clastic sequences of Miocene age. The fissures show a wide range of orientations, but consistently display north–south opening vectors and are almost certainly related to opening of the nearby Catanzaro graben, which was associated with extension in the Tyrrhenian back-arc region. A small proportion of the finer grained fissure-fills found in the deeper parts of the basement show evidence consistent with hydraulic sediment injection. Overpressure and sediment remobilization were most likely driven by the seismicity accompanying rift-related regional fault activity.

Naturally propped, deeply penetrating fissures of this kind have the potential to form a voluminous and highly interconnected network of significantly porous and permeable void spaces developed in otherwise impermeable basement host rocks. They can therefore act as significant fluid migration channel ways and also have the capacity to form an excellent fluid reservoir in their own right for hydrocarbons, water or hydrothermal fluids. In areas where contemporaneous cover sequences have subsequently been eroded, the fissure-fills also provide information on the near-surface geological and tectonic history during sedimentary basin formation that may otherwise be missing from the rock record. We suggest that the development of sub-unconformity fissure-fill systems of this kind has been underestimated in ancient settings and that further exploration of these geologically complex fracture arrays in near-surface settings is warranted.

*Scientific editing by Matias Ghiglione*

**Acknowledgements** We thank Christine Siddoway for earlier discussions and enthusiastic participation in earlier fieldwork in the Copanello–Pietragrande area. Constructive reviews by Lars Riber, Nigel Woodcock and Editor Matias Ghiglione were very much appreciated.

**Author contributions** KH: data curation (lead), formal analysis (lead), investigation (lead), visualization (lead), writing – original draft (lead); REH: conceptualization (lead), methodology (lead), supervision (lead), writing –

review & editing (lead); **GP**: conceptualization (supporting), data curation (supporting), formal analysis (supporting), investigation (supporting), investigation (supporting), writing – review & editing (supporting), writing – review & editing (supporting); **GP**: conceptualization (supporting), data curation (supporting), formal analysis (supporting), investigation (supporting), investigation (supporting), writing – review & editing (supporting), writing – review & editing (supporting); **ZK**: investigation (supporting), writing – review & editing (supporting); **KJWM**: methodology (supporting), supervision (supporting), writing – review & editing (supporting).

**Funding** This research received no specific grant from any funding agency in the public, commercial, or not-for-profit sectors. KH was a self-funded PhD student.

**Competing interests** The authors declare that they have no known competing financial interests or personal relationships that could have appeared to influence the work reported in this paper.

**Data availability** All data generated or analysed during this study are included in this published article.

## References

- Angelier, J. 1991. Inversion directe et recherche 4-D: comparaison physique et mathématique de deux modes de détermination des tenseurs des paleocontraintes en tectonique de failles. *Comptes Rendus – Académie des Sciences, Série II*, **312**, 1213–1218.
- Angelier, J. and Mechler, P. 1977. Sur une méthode graphique de recherche des contraintes principales également utilisables en tectonique et en séismologie: la méthode des dièdres droits. *Bulletin de la Société Géologique de France*, **S7-XIX**, 1309–1318, <https://doi.org/10.2113/gssgfbull.S7-XIX.6.1309>
- Bemis, S.P., Micklethwaite, S., Turner, D., James, M.R., Akciz, S., Thiele, S.T. and Bangash, H.A. 2014. Ground-based and UAV-based photogrammetry: a multi-scale, high-resolution mapping tool for structural geology and paleoseismology. *Journal of Structural Geology*, **69**, 163–178, <https://doi.org/10.1016/j.jsg.2014.10.007>
- Biddle, K.T. and Wielchowsky, C.C. 1994. Hydrocarbon traps: chapter 13: part III. Processes. In: Magoon, L. and Dow, W. (eds) *The Petroleum System – From Source To Trap*. AAPG, Memoirs, **60**, 219–235.
- Bonardi, G., Cavazza, W., Perrone, V. and Rossi, S. 2001. Calabria–Peloritani terrane and northern Ionian Sea. In: Vai, G.B. and Martini, I.P. (eds) *Anatomy of an Orogen: the Apennines and Adjacent Mediterranean Basins*. Springer, Dordrecht, 287–306, [https://doi.org/10.1007/978-94-015-9829-3\\_17](https://doi.org/10.1007/978-94-015-9829-3_17)
- Borrelli, L., Coniglio, S., Critelli, S., La Barbera, A. and Gullà, G. 2016. Weathering grade in granitoid rocks: the San Giovanni in Fiore area. *Journal of Maps*, **12**, 260–275, <https://doi.org/10.1080/17445647.2015.1010742>
- Bott, M.H.P. 1959. The mechanics of oblique slip faulting. *Geological Magazine*, **XCVI**, 109–117, <https://doi.org/10.1017/S0016756800059987>
- Brutto, F., Muto, F., Loreto, M.F., Paola, N. De, Tripodi, V., Critelli, S. and Facchin, L. 2016. The Neogene–Quaternary geodynamic evolution of the central Calabrian Arc: a case study from the western Catanzaro Trough basin. *Journal of Geodynamics*, **102**, 95–114, <https://doi.org/10.1016/j.jog.2016.09.002>
- Caggianelli, A. and Di Florio, M.R. 1989. Trondhjemitic evolution caused by compaction of a crystal mush: an example from Southern Calabria (Italy). *Periodico di Mineralogia*, **58**, 9–23.
- Caggianelli, A., Prosser, G. and Rottura, A. 2000. Thermal history vs. fabric anisotropy in granitoids emplaced at different crustal levels: an example from Calabria, southern Italy. *Terra Nova*, **12**, 109–116, <https://doi.org/10.1046/j.1365-3121.2000.123280.x>
- Caggianelli, A., Lorenzo, S. and Prosser, G. 2005. Modelling the heat pulses generated on a fault plane during coseismic slip: inferences from the pseudotachylites of the Copanello cliffs (Calabria, Italy). *Tectonophysics*, **405**, 99–119, <https://doi.org/10.1016/j.tecto.2005.05.017>
- Cavazza, W., Blenkinsop, J., DeCelles, P., Patterson, R.T. and Reinhardt, E.D. 1997. Stratigrafia e sedimentologia della sequenza sedimentaria Oligocenico–Quaternaria del Bacino Calabro-Ionico. *Bollettino della Società Geologica Italiana*, **116**, 51–77.
- Ceccato, A., Viola, G., Tartaglia, G. and Antonellini, M. 2021. In-situ quantification of mechanical and permeability properties on outcrop analogues of offshore fractured and weathered crystalline basement: examples from the Rolvsnes granodiorite, Bomlo, Norway. *Marine and Petroleum Geology*, **124**, 104859, <https://doi.org/10.1016/j.marpetgeo.2020.104859>
- Cirriacione, R., Fazio, E., Fiannacca, P., Ortolano, G., Pezzino, A. and Punturo, R. 2015. The Calabria–Peloritani Orogen, a composite terrane in Central Mediterranean; its overall architecture and geodynamic significance for a pre-Alpine scenario around the Tethyan basin. *Periodico di Mineralogia*, **84**, 701–749, <https://doi.org/10.2451/2015PM0446>
- Cornée, J.J., Münch, P. *et al.* 2016. The Messinian erosional surface and early Pliocene reflooding in the Alboran Sea: new insights from the Boudinar basin, Morocco. *Sedimentary Geology*, **333**, 115–129, <https://doi.org/10.1016/j.sedgeo.2015.12.014>
- Cox, S.F. and Etheridge, M.A. 1983. Crack-seal fibre growth mechanisms and their significance in the development of oriented layer silicate microstructures. *Tectonophysics*, **92**, 147–170, [https://doi.org/10.1016/0040-1951\(83\)90088-4](https://doi.org/10.1016/0040-1951(83)90088-4)
- Cox, S.F. and Munroe, S.M. 2016. Breccia formation by particle fluidization in fault zones: implications for transitory, rupture-controlled fluid flow regimes in hydrothermal systems. *American Journal of Science*, **316**, 241–278, <https://doi.org/10.2475/03.2016.02>
- Cuong, T.X. and Warren, J.K. 2009. Bach Ho field, a fractured granitic basement reservoir, Cuu Long Basin, offshore SE Vietnam: a ‘buried-hill’ play. *Journal of Petroleum Geology*, **32**, 129–156, <https://doi.org/10.1111/j.1747-5457.2009.00440.x>
- Delvaux, D. and Sperner, B. 2003. New aspects of tectonic stress inversion with reference to the TENSOR program. *Geological Society, London, Special Publications*, **212**, 75–100, <https://doi.org/10.1144/GSL.SP.2003.212.01.06>
- Delvaux, D., Moeys, R., Stapel, G., Melnikov, A. and Ermikov, V. 1995. Palaeostress reconstructions and geodynamics of the Baikal region, Central Asia, Part I. Palaeozoic and Mesozoic pre-rift evolution. *Tectonophysics*, **252**, 61–101, [https://doi.org/10.1016/0040-1951\(95\)00090-9](https://doi.org/10.1016/0040-1951(95)00090-9)
- Dowey, P.J., Worden, R.H., Utley, J. and Hodgson, D.M. 2017. Sedimentary controls on modern sand grain coat formation. *Sedimentary Geology*, **353**, 46–63, <https://doi.org/10.1016/j.sedgeo.2017.03.001>
- Finetti, I.R. and Del Ben, A. 1986. Geophysical study of the Tyrrhenian Opening. *Bollettino di Geofisica Teorica ed Applicata*, **110**, 75–156.
- Flood, R.D. 1981. Distribution, morphology, and origin of sedimentary furrows in cohesive sediments, Southampton Water. *Sedimentology*, **28**, 511–529, <https://doi.org/10.1111/j.1365-3091.1981.tb01699.x>
- Frenzel, M. and Woodcock, N.H. 2014. Cockade breccia: product of mineralisation along dilational faults. *Journal of Structural Geology*, **68**, 194–206, <https://doi.org/10.1016/j.jsg.2014.09.001>
- Ghissetti, F. and Vezzani, L. 1981. Contribution of structural analysis to understanding the geodynamic evolution of the Calabrian Arc (Southern Italy). *Journal of Structural Geology*, **3**, 371–381, [https://doi.org/10.1016/0191-8141\(81\)90037-7](https://doi.org/10.1016/0191-8141(81)90037-7)
- Guido, A., Jacob, J., Gautret, P., Laggoun-Défarage, F., Mastan-Drea, A. and Russo, F. 2007. Molecular fossils and other organic markers as palaeoenvironmental indicators of the Messinian Cal-care di Base Formation: normal versus stressed marine deposition (Rossano Basin, northern Calabria, Italy). *Palaeogeography, Palaeoclimatology, Palaeoecology*, **255**, 265–283, <https://doi.org/10.1016/j.palaeo.2007.07.015>
- Gutmanis, J.C. 2009. Basement reservoirs – a review of their geological and production histories. In: *International Petroleum Technology Conference*, Doha, Qatar, 7–9 December, IPTC 13156, <https://doi.org/10.2523/IPTC-13156-MS>
- Hardman, K. 2020. *Fault Void Fills: Pervasive and Persistent Fluid Flow Pathways in Fractured Crystalline and Carbonate Reservoirs*. PhD thesis, Durham University, <http://theses.dur.ac.uk/13911/>
- Hardman, K., Holdsworth, R.E., Dempsey, E. and McCaffrey, K. 2020. The nature and significance of rift-related, near-surface fissure fill networks in fractured carbonates below regional unconformities. *Journal of the Geological Society, London*, **177**, 1168–1185, <https://doi.org/10.1144/jgs2020-074>
- Holdsworth, R.E., McCaffrey, K.J.W. *et al.* 2019. Natural fracture propping and earthquake-induced oil migration in fractured basement reservoirs. *Geology*, **47**, 700–704, <https://doi.org/10.1130/G46280.1>
- Holdsworth, R.E., Trice, R. *et al.* 2020. The nature and age of basement host rocks and fissure fills in the Lancaster field fractured reservoir, west of Shetland. *Journal of the Geological Society, London*, **177**, 1057–1073, <https://doi.org/10.1144/jgs2019-142>
- Holland, M., Van Gent, H.W., Bazalgette, L., Yassir, N., Hoogerduijn-Strating, E.H. and Urai, J.L. 2011. Evolution of dilatant fracture networks in normal faults – evidence from 4D model experiments. *Earth and Planetary Sciences Letters*, **304**, 399–406, <https://doi.org/10.1016/j.epsl.2011.02.017>
- Hurst, A., Scott, A. and Vigorito, M. 2011. Physical characteristics of sand injectites. *Earth-Science Reviews*, **106**, 215–246, <https://doi.org/10.1016/j.earscirev.2011.02.004>
- Hutton, D.H.W. 1988. Granite emplacement mechanisms and tectonic controls: inferences from deformation studies. *Transactions of the Royal Society of Edinburgh: Earth Sciences*, **79**, 245–255, <https://doi.org/10.1017/S0263593300014255>
- Letto, A. and Letto, F. 2004. Age and history of the weathering of granitoids in southern Calabria (Italy). *Geografia Fisica e Dinamica Quaternaria*, **27**, 37–45.
- Jonk, R. 2010. Sand-rich injectites in the context of short-lived and long-lived fluid flow. *Basin Research*, **22**, 603–621, <https://doi.org/10.1111/j.1365-2117.2010.00471.x>
- Jonk, R., Duranti, D., Parnell, J., Hurst, A. and Fallick, A.E. 2003. The structural and diagenetic evolution of injected sandstones: examples from the Kimmeridgian of NE Scotland. *Journal of the Geological Society, London*, **160**, 881–894, <https://doi.org/10.1144/0016-764902-091>
- Langone, A., Caggianelli, A., Festa, V. and Prosser, G. 2014. Time constraints on the building of the Serre batholith: consequences for the thermal evolution of the Hercynian continental crust exposed in Calabria (Southern Italy). *Journal of Geology*, **122**, 183–199, <https://doi.org/10.1086/675227>
- Lachassagne, P., Dewandel, B. and Wyns, R. 2021. Review: hydrogeology of weathered crystalline/hard-rock aquifers – guidelines for the operational survey and management of their groundwater resources. *Hydrogeology Journal*, **29**, 2561–2594, <https://doi.org/10.1007/s10040-021-02339-7>

- Le Pera, E. and Sorriso-Valvo, M. 2000. Weathering and morphogenesis in a Mediterranean climate, Calabria, Italy. *Geomorphology*, **34**, 251–270, [https://doi.org/10.1016/S0169-555X\(00\)00012-X](https://doi.org/10.1016/S0169-555X(00)00012-X)
- Massari, F. and Prosser, G. 2013. Late Cenozoic tectono-stratigraphic sequences of the Crotona Basin: insights on the geodynamic history of the Calabrian arc and Tyrrhenian Sea. *Basin Research*, **25**, 26–51, <https://doi.org/10.1111/j.1365-2117.2012.00549.x>
- Massari, F., Prosser, G., Capraro, L., Fornaciari, E. and Consolaro, C. 2010. A revision of the stratigraphy and geology of the south-western part of the Crotona Basin (South Italy). *Italian Journal of Geosciences*, **129**, 353–384, <https://doi.org/10.3301/IJG.2010.20>
- McCaffrey, K.J.W., Holdsworth, R.E., Pless, J., Franklin, B.S.G. and Hardman, K. 2020. Basement reservoir plumbing: fracture aperture, length and topology analysis of the Lewisian Complex, NW Scotland. *Journal of the Geological Society, London*, **177**, 1281–1293, <https://doi.org/10.1144/jgs2019-143>
- Minelli, L., Vecchio, A. *et al.* 2016. Aeromagnetic investigation of southern Calabria and the Messina Straits (Italy): tracking seismogenic sources of 1783 and 1908 earthquakes. *Journal of Geophysical Research: Solid Earth*, **121**, 1297–1315, <https://doi.org/10.1002/2015JB012305>
- Monaco, C., Tortorici, L., Nicolich, R., Cernobori, L. and Costa, M. 1996. From collisional to rifted basins: an example from the southern Calabrian arc (Italy). *Tectonophysics*, **266**, 233–249, [https://doi.org/10.1016/S0040-1951\(96\)00192-8](https://doi.org/10.1016/S0040-1951(96)00192-8)
- Montenan, C., Barrier, P. and D'Esteveou, P.O. 1991. Some aspects of the recent tectonics in the Strait of Messina, Italy. *Tectonophysics*, **194**, 203–215, [https://doi.org/10.1016/0040-1951\(91\)90261-P](https://doi.org/10.1016/0040-1951(91)90261-P)
- Ortega, O.J., Marrett, R.A. and Laubach, S.E. 2006. A scale-independent approach to fracture intensity and average spacing measurement. *AAPG Bulletin*, **90**, 193–208, <https://doi.org/10.1306/08250505059>
- Ortolano, G., Visalli, R. *et al.* 2020. Tectono-metamorphic evolution of the Calabria continental lower crust: the case of the Sila Piccola Massif. *International Journal of Earth Sciences*, **109**, 1295–1319, <https://doi.org/10.1007/s00531-020-01873-1>
- Palladino, G., Grippa, A., Bureau, D., Alsop, G.I. and Hurst, A. 2016. Emplacement of sandstone intrusions during contractional tectonics. *Journal of Structural Geology*, **89**, 230–249, <https://doi.org/10.1016/j.jsg.2016.06.010>
- Palladino, G., Alsop, G.I., Grippa, A., Zvirtes, G., Phillip, R.P. and Hurst, A. 2018. Sandstone-filled normal faults: a case study from central California. *Journal of Structural Geology*, **110**, 86–101, <https://doi.org/10.1016/j.jsg.2018.02.013>
- Palladino, G., Alsop, G.I., Grippa, A., Seers, T. and Hurst, A. 2021. Sandstone intrusions along different types of faults and their effect on fluid flow in siliciclastic reservoirs. *Geological Society, London, Special Publications*, **493**, 273–286, <https://doi.org/10.1144/SP493-2018-45>
- Petit, J.P. 1987. Criteria for the sense of movement on fault surfaces in brittle rocks. *Journal of Structural Geology*, **9**, 597–608, [https://doi.org/10.1016/0191-8141\(87\)90145-3](https://doi.org/10.1016/0191-8141(87)90145-3)
- Riber, L., Dypvik, H. and Sørli, R. 2015. Altered basement rocks on the Utsira High and its surroundings, Norwegian North Sea. *Norwegian Journal of Geology*, **95**, 57–89, <https://doi.org/10.17850/njg95-1-04>
- Riber, L., Dypvik, H., Sørli, R., Naqvis, A.M., Stangvik, K., Oberhardt, N. and Schroeder, P.A. 2017. Comparison of deeply buried palaeoregolith profiles, Norwegian North Sea, with outcrops from southern Sweden and Georgia, USA – implications for petroleum exploration. *Palaeogeography, Palaeoclimatology, Palaeoecology*, **471**, 82–95, <https://doi.org/10.1016/j.palaeo.2017.01.043>
- Richter, D. 1966. On the New Red Sandstone Neptunian dykes of the Tor Bay area (Devonshire). *Proceedings of the Geologists' Association*, **77**, 173–186, [https://doi.org/10.1016/S0016-7878\(66\)80068-8](https://doi.org/10.1016/S0016-7878(66)80068-8)
- Rossetti, F., Goffé, B., Monié, P., Faccenna, C. and Vignaroli, G. 2004. Alpine orogenic P–T–t-deformation history of the Catena Costiera area and surrounding regions (Calabrian Arc, southern Italy): the nappe edifice of north Calabria revised with insights on the Tyrrhenian–Apennine system formation. *Tectonics*, **23**, 1–26, <https://doi.org/10.1029/2003TC001560>
- Rowe, C.D., Ross, C. *et al.* 2018. Geometric complexity of earthquake rupture surfaces preserved in pseudotachylyte networks. *Journal of Geophysical Research: Solid Earth*, **123**, 7998–8015, <https://doi.org/10.1029/2018JB016192>
- Sanderson, D.J. and Nixon, C.W. 2015. The use of topology in fracture network characterization. *Journal of Structural Geology*, **72**, 55–66, <https://doi.org/10.1016/j.jsg.2015.01.005>
- Schenk, V. 1990. The exposed crustal cross section of southern Calabria, Italy: structure and evolution of a segment of Hercynian crust. *In: Salisbury, M.H. and Fountain, D.M. (eds) Exposed Cross-sections of the Continental Crust*. Kluwer, Dordrecht, 21–42.
- Sibson, R.H. 1994. Crustal stress, faulting and fluid flow. *Geological Society, London, Special Publications*, **78**, 69–84, <https://doi.org/10.1144/GSL.SP.1994.078.01.07>
- Siddoway, C.S. and Gehrels, G.E. 2014. Basement-hosted sandstone injectites of Colorado: a vestige of the Neoproterozoic revealed through detrital zircon provenance analysis. *Lithosphere*, **6**, 403–408, <https://doi.org/10.1130/L390.1>
- Siddoway, C.S., Palladino, G., Prosser, G., Freedman, D. and Duckworth, W.C. 2019. Basement-hosted sand injectites: use of field examples to advance understanding of hydrocarbon reservoirs in fractured crystalline basement rocks. *Geological Society, London, Special Publications*, **493**, 215–233, <https://doi.org/10.1144/SP493-2018-140>
- Spina, V., Tondi, E. and Mazzoli, S. 2011. Complex basin development in a wrench-dominated back-arc area: tectonic evolution of the Crati Basin, Calabria, Italy. *Journal of Geodynamics*, **51**, 90–109, <https://doi.org/10.1016/j.jjog.2010.05.003>
- Thomson, S.N. 1994. Fission track analysis of the crystalline basement rocks of the Calabrian Arc, southern Italy: evidence of Oligo-Miocene late-orogenic extension and erosion. *Tectonophysics*, **238**, 331–352, [https://doi.org/10.1016/0040-1951\(94\)90063-9](https://doi.org/10.1016/0040-1951(94)90063-9)
- Tribe, I.R. and D'Lemos, R.S. 1996. Significance of a hiatus in down-temperature fabric development within syntectonic quartz diorite complexes, Channel Islands, UK. *Journal of the Geological Society, London*, **153**, 127–138, <https://doi.org/10.1144/gsjgs.153.1.0127>
- Trice, R. 2014. Basement exploration West of Shetlands, progress in opening a new play on the UKCS. *Geological Society, London, Special Publications*, **397**, 81–105, <https://doi.org/10.1144/SP397.3>
- Trice, R., Hiorth, C. and Holdsworth, R.E. 2019. Fractured basement play development in the UK and Norwegian rifted margins: a discussion and implications for exploitation. *Geological Society, London, Special Publications*, **495**, <https://doi.org/10.1144/SP495-2018-174>
- Tripodi, V., Muto, F., Brutto, F., Perri, F. and Critelli, S. 2018. Neogene–Quaternary evolution of the forearc and backarc regions between the Serre and Aspromonte Massifs, Calabria (southern Italy). *Marine and Petroleum Geology*, **95**, 328–343, <https://doi.org/10.1016/j.marpetgeo.2018.03.028>
- Ullman, S. 1979. The interpretation of structure from motion. *Proceedings of the Royal Society of London B: Biological Sciences*, **203**, 405–426, <https://doi.org/10.1098/rspb.1979.0006>
- van Dijk, J.P., Bello, M. *et al.* 2000. A regional structural model for the northern sector of the Calabrian Arc (southern Italy). *Tectonophysics*, **324**, 267–320, [https://doi.org/10.1016/S0040-1951\(00\)00139-6](https://doi.org/10.1016/S0040-1951(00)00139-6)
- van Gent, H.W., Holland, M., Urai, J.L. and Loosveld, R. 2010. Evolution of fault zones in carbonates with mechanical stratigraphy – insights from scale models using layered cohesive powder. *Journal of Structural Geology*, **32**, 1375–1391, <https://doi.org/10.1016/j.jsg.2009.05.006>
- Vidal, J. and Genter, A. 2018. Overview of naturally permeable fractured reservoirs in the central and southern Upper Rhine Graben: insights from geothermal wells. *Geothermics*, **74**, 57–73, <https://doi.org/10.1016/j.geothermics.2018.02.003>
- von Hagke, C., Kettermann, M., Bitsch, N., Bücken, D., Weismüller, C. and Urai, J.L. 2019. The effect of obliquity of slip in normal faults on distribution of open fractures. *Frontiers in Earth Science*, **7**, 18, <https://doi.org/10.3389/feart.2019.00018>
- Walker, R.J., Holdsworth, R.E., Imber, J. and Ellis, D. 2011. The development of cavities and clastic infills along fault-related fractures in Tertiary basalts on the NE Atlantic margin. *Journal of Structural Geology*, **33**, 92–106, <https://doi.org/10.1016/j.jsg.2010.12.001>
- Wallace, R.E. 1951. Geometry of shearing stress and relation to faulting. *The Journal of Geology*, **59**, 118–130, <https://doi.org/10.1086/625831>
- Weismüller, C., Urai, J.L., Kettermann, M., von Hagke, C. and Reicherter, K. 2019. Structure of massively dilatant faults in Iceland: lessons learned from high-resolution unmanned aerial vehicle data. *Solid Earth*, **10**, 1757–1784, <https://doi.org/10.5194/se-10-1757-2019>
- Woodcock, N.H., Miller, A.V.M. and Woodhouse, C.D. 2014. Chaotic breccia zones on the Pembroke Peninsula, south Wales: evidence for collapse into voids along dilational faults. *Journal of Structural Geology*, **69**, 91–107, <https://doi.org/10.1016/j.jsg.2014.09.019>
- Wright, V., Woodcock, N.H. and Dickson, J.A.D. 2009. Fissure fills along faults: Variscan examples from Gower, South Wales. *Geological Magazine*, **146**, 890–902, <https://doi.org/10.1017/S001675680999001X>
- Zecchin, M., Caffau, M. *et al.* 2012. The Plio-Pleistocene evolution of the Crotona Basin (southern Italy): interplay between sedimentation, tectonics and eustasy in the frame of Calabrian Arc migration. *Earth-Science Reviews*, **115**, 273–303, <https://doi.org/10.1016/j.earscirev.2012.10.005>